

---

# Dynamic Likelihood-free Inference via Ratio Estimation (DIRE)

---

**Traiko Dinev**

School of Informatics  
University of Edinburgh  
traiko.dinev@ed.ac.uk

**Michael U. Gutmann**

School of Informatics  
University of Edinburgh  
michael.gutmann@ed.ac.uk

## Abstract

Parametric statistical models that are implicitly defined in terms of a stochastic data generating process are used in a wide range of scientific disciplines because they enable accurate modeling. However, learning the parameters from observed data is generally very difficult because their likelihood function is typically intractable. Likelihood-free Bayesian inference methods have been proposed which include the frameworks of approximate Bayesian computation (ABC), synthetic likelihood, and its recent generalization that performs likelihood-free inference by ratio estimation (LFIRE). A major difficulty in all these methods is choosing summary statistics that reduce the dimensionality of the data to facilitate inference. While several methods for choosing summary statistics have been proposed for ABC, the literature for synthetic likelihood and LFIRE is very thin to date. We here address this gap in the literature, focusing on the important special case of time-series models. We show that convolutional neural networks trained to predict the input parameters from the data provide suitable summary statistics for LFIRE. On a wide range of time-series models, a single neural network architecture produced equally or more accurate posteriors than alternative methods.

## 1 Introduction

We consider the task of estimating the posterior density  $p(\boldsymbol{\theta} \mid \mathbf{x}^o)$  of parameters  $\boldsymbol{\theta}$  given observed data  $\mathbf{x}^o$  when the statistical model  $p(\mathbf{x} \mid \boldsymbol{\theta})$  is implicitly specified in terms of a stochastic computer program that takes the model parameters  $\boldsymbol{\theta}$  as input and gen-

erates samples  $\mathbf{x}$  from  $p(\mathbf{x} \mid \boldsymbol{\theta})$  as output. Such models enable accurate modeling of possibly nonlinear stochastic phenomena and are widely used in scientific disciplines as diverse as genetics (Tavaré et al. 1997; Arnold et al. 2018), physics (Cameron and Pettitt 2012; Tietäväinen et al. 2017), ecology and evolution (Hartig et al. 2011; Corander et al. 2017), econometrics (Gouriéroux and Monfort 1996; Frazier et al. 2018), and vision and robotics (Mansinghka et al. 2013; Lopez-Guevara et al. 2017).

While the computer program enables us to generate samples from  $p(\mathbf{x} \mid \boldsymbol{\theta})$ , it does not provide us with a direct way of evaluating  $p(\mathbf{x} \mid \boldsymbol{\theta})$  — the models are thus said to be implicitly defined (Diggle and Gratton 1984). Moreover, numerical evaluation of  $p(\mathbf{x} \mid \boldsymbol{\theta})$  for all but the simplest implicit models is prohibitively expensive, which means that the likelihood function  $L(\boldsymbol{\theta}) = p(\mathbf{x}^o \mid \boldsymbol{\theta})$  is not available either and estimating the posterior becomes very difficult.

Several likelihood-free Bayesian inference methods to estimate the posterior exist when only sampling from the model is possible. The methods include approximate Bayesian computation (ABC, Tavaré et al. 1997; Pritchard et al. 1999), synthetic likelihood (Wood 2010; Price et al. 2017) and its generalizations (Dutta et al. 2016; Fasiolo et al. 2018); for recent reviews, see e.g. (Lintusaari et al. 2017; Sisson et al. 2018). The methods rely on summary statistics  $\Psi$  that reduce the dimensionality of the data. ABC uses the summary statistics to assess the similarity between the simulated and observed data (by typically computing the Euclidean distance between them), while the synthetic likelihood approach models the summary statistics as a Gaussian distribution for each parameter value; its generalizations relax the Gaussianity assumption.

The summary statistics thus crucially affect the estimated posterior. In ABC, there has been considerable work on learning or selecting suitable summaries using dimensionality reduction methods and methods from

regression and classification (see e.g. Aeschbacher et al. 2012; Fearnhead and Prangle 2012; Blum et al. 2013; Gutmann et al. 2018; Jiang et al. 2018). But for the synthetic likelihood approach and its generalizations, the literature is very thin to date.

To evaluate the synthetic likelihood pointwise at a value of  $\theta$ , we have to estimate and invert the covariance matrix of the summary statistics, which can pose numerical challenges. Robust methods have been proposed that can be considered to correspond to some form of summary statistics selection or transformation: Wood (2010) proposes preconditioning and reweighting of the summary statistics, Ong et al. (2017) uses shrinkage estimation of the covariance matrix and An et al. (2018) the graphical lasso to obtain sparse estimates of its inverse. In the generalization of the synthetic likelihood by Dutta et al. (2016), named likelihood-free inference by ratio estimation (LFIRE), the authors use their method to automatically select and combine relevant summary statistics from a larger pool of candidates. But much like the aforementioned approaches for the synthetic likelihood, it is assumed that the list of candidate summary statistics contains suitable ones in the first place.

The aim of this article is to lift this burden on the user and to enhance LFIRE with a practical method that automatically learns suitable summary statistics from the raw data  $\mathbf{x}$ . We propose that predicted parameter values, computed directly from the raw data, provide summaries that are well suited for LFIRE. Focusing on the special but important case of time-series data and stochastic dynamical models, we show that convolutional neural networks are particularly apt to learn such summary statistics for LFIRE.

The rest of the article is structured as follows. Section 2 explains the proposed approach and Section 3 validates the method on models where the posterior can be accurately computed. In Section 4, we apply it to complex models with intractable likelihoods, and Section 5 concludes the paper.

## 2 Learning summary statistics for LFIRE on time-series data

We first review LFIRE and discuss which summary statistics are suitable for this likelihood-free inference framework. We then propose to learn them for time-series data by using convolutional neural networks and then present the proposed method.

### 2.1 Summary statistics for LFIRE

The LFIRE approach of Dutta et al. (2016) formulates the problem of posterior density estimation as

a problem of estimating the ratio  $r(\theta, \mathbf{x})$  between the data generating distribution  $p(\mathbf{x} | \theta)$  and the marginal  $p(\mathbf{x}) = \int p(\mathbf{x} | \theta)\pi(\theta) d\theta$ , where  $\pi(\theta)$  is the prior over  $\theta$ .<sup>1</sup> After the ratio is estimated, the posterior follows directly from Bayes' theorem,

$$p(\theta | \mathbf{x}^o) = r(\theta, \mathbf{x}^o)\pi(\theta), \quad r(\theta, \mathbf{x}) = \frac{p(\mathbf{x} | \theta)}{p(\mathbf{x})}. \quad (1)$$

For models specified by a data generating process, we cannot evaluate  $p(\mathbf{x} | \theta)$  and  $p(\mathbf{x})$  but we can sample from the two distributions.<sup>2</sup> This is exploited by Dutta et al. (2016) who estimate the ratio  $r(\theta, \mathbf{x})$  by training a logistic regression model to learn to classify between data sampled from  $p(\mathbf{x} | \theta)$  and  $p(\mathbf{x})$  (other methods to estimate the ratio can also be used, see Gutmann and Hirayama 2011; Sugiyama et al. 2012).

In more detail, let  $\mathcal{X}_\theta = \{\mathbf{x}_\theta^{(i)}\}$  be a set of  $n_\theta$  samples from  $p(\mathbf{x} | \theta)$ ,  $\mathcal{X}_m = \{\mathbf{x}_m^{(i)}\}$  a set of  $n_m$  samples from  $p(\mathbf{x})$ , and  $h_\beta(\mathbf{x})$  a parametric model for  $\log r(\theta, \mathbf{x})$  for any given value of  $\theta$ . Dutta et al. (2016) learn the value of the log ratio at  $\theta$  by minimizing the logistic loss

$$\mathcal{L}_\theta(\beta) = \frac{1}{n} \left\{ \sum_{i=1}^{n_\theta} \log \left[ 1 + \nu \exp(-h_\beta(\mathbf{x}_\theta^{(i)})) \right] + \sum_{i=1}^{n_m} \log \left[ 1 + \frac{1}{\nu} \exp(h_\beta(\mathbf{x}_m^{(i)})) \right] \right\} + \Omega(\beta) \quad (2)$$

with respect to  $\beta$ , where  $\Omega(\beta)$  is a regularizing penalty term.<sup>3</sup> While other parametrizations of  $h_\beta(\mathbf{x})$  are possible, for their empirical results, Dutta et al. (2016) worked with

$$h_\beta(\mathbf{x}) = \beta^\top \Psi(\mathbf{x}) \quad (3)$$

where  $\Psi(\mathbf{x})$  is a fixed vector-valued nonlinear transformation of the raw data  $\mathbf{x}$ . They are the features in the classification problem and correspond to summary statistics in likelihood-free inference. Dutta et al. (2016) selected and combined the relevant ones by using the  $L_1$  penalty  $\Omega(\beta) = \lambda \sum_i |\beta_i|$  together with cross-validation to choose the penalty strength  $\lambda$ .

The issue of choosing summary statistics in likelihood-free inference manifests itself in the LFIRE framework in the question of how to model  $\log r(\theta, \mathbf{x})$ , or equivalently, which features to choose for classification. Ideally, we would like to have features for which classification can be performed with a simple decision boundary in the feature space. Our approach to generate

<sup>1</sup>A related approach for estimating likelihood-ratios can be found in (Cranmer et al. 2015).

<sup>2</sup>To sample from the marginal  $p(\mathbf{x})$ , we first sample a  $\theta'$  from the prior and then a  $\mathbf{x}$  from  $p(\mathbf{x} | \theta')$ .

<sup>3</sup>After learning,  $\hat{\beta}(\theta) = \operatorname{argmin}_\beta \mathcal{L}_\theta(\beta)$  and  $\hat{h}(\theta, \mathbf{x}) = h_{\hat{\beta}(\theta)}(\mathbf{x}) \approx \log r(\theta, \mathbf{x})$ .

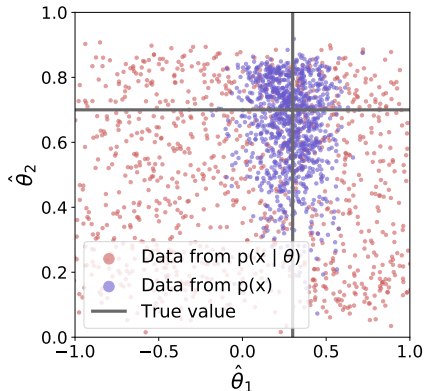


Figure 1: We propose to use predictors  $\hat{\theta}(\mathbf{x})$  to define the summary statistics for LFIRE. For  $\mathbf{x} \sim p(\mathbf{x} | \boldsymbol{\theta})$ , here  $\boldsymbol{\theta} = (0.3, 0.7)$ , the predictions are concentrated around  $\boldsymbol{\theta}$  (blue) while for  $\mathbf{x} \sim p(\mathbf{x})$ , the predictions are spread out in the parameter space (red). An elliptic decision boundary can be used to classify the two data clouds and hence to learn the ratio  $r(\boldsymbol{\theta}, \mathbf{x})$  in (1).

summary statistics for LFIRE thus consists in learning features for which the decision boundary has a particularly simple form.

The main idea is that features (summary statistics) that are suitable for LFIRE can be learned by inverting the data process, that is, by learning to predict the value of  $\boldsymbol{\theta}$  from the data  $\mathbf{x}$ . The learned predictors  $\hat{\theta}(\mathbf{x})$  then define the desired summary statistics for LFIRE. Indeed, if the learning is done well, the predictions based on  $\mathbf{x} \sim p(\mathbf{x} | \boldsymbol{\theta})$  will cluster around  $\boldsymbol{\theta}$  while the predictions based on  $\mathbf{x} \sim p(\mathbf{x})$  are spread out over the domain of the prior so that a simple elliptical decision boundary can be used to perform the classification. This means that we can work with a parametric model  $h_{\beta}(\mathbf{x})$  as in (3) where  $\Psi(\mathbf{x})$  is given by the predicted parameter values  $\hat{\theta}_i(\mathbf{x})$  as well as all their squares and unique pair-wise combinations and a constant, i.e. for a  $d$ -dimensional parameter space

$$\Psi = (\hat{\theta}_1, \dots, \hat{\theta}_d, \hat{\theta}_1^2, \hat{\theta}_1\hat{\theta}_2, \dots, \hat{\theta}_{d-1}\hat{\theta}_d, \hat{\theta}_d^2, 1) \quad (4)$$

where we suppressed the dependency on  $\mathbf{x}$ . Figure 1 illustrates this idea for the ARCH model (see below).

## 2.2 Learning summary statistics for time-series data

The predictors  $\hat{\theta}(\mathbf{x})$  can be learned from parameter-data pairs  $(\boldsymbol{\theta}, \mathbf{x})$  with  $\mathbf{x} \sim p(\mathbf{x} | \boldsymbol{\theta})$  by (nonlinear) regression, and neural networks provide a very flexible function class among which to search for the predictors. Importantly, however, no single network architecture and training method will work for all kinds of data. Since we would like to learn the predictors

with as little user guidance and manual tuning as possible, we focus on time-series data where the popular convolutional networks provide a restricted yet flexible enough function class.

Convolutional networks have fewer parameters to learn and are suited for describing time-series data because they can capture higher-order statistical dependencies between different time points. Related (nonlinear) autocorrelation functions have been used as summary statistics in previous work (e.g. Wood 2010). We will see that a *single* generic neural network architecture is able to produce suitable summary statistics for LFIRE on a range of different time-series models and data sets.

Neural networks have been used before in ABC: Blum and Francois (2010); Papamakarios and Murray (2016) used them in the context of regression ABC where the summary statistics are assumed to be given, and, more relevant for the topic of this paper, Jiang et al. (2018) used them to learn summary statistics from raw data for use in ABC. The main difference of the latter work to this paper is (a) the different likelihood-free inference framework — ABC versus LFIRE and (b) the focus on time-series and the use of convolutional neural networks.

## 2.3 Proposed method

In line with the above, the proposed method to enhance LFIRE with summary statistics for time-series data separates into two distinct stages. The first is to train a convolutional neural network to predict  $\boldsymbol{\theta}$  from  $\mathbf{x}$ . The second is to run LFIRE with the model  $h_{\beta}(\mathbf{x})$  for the log-ratio in (3) and summary statistics defined by the learned predictors  $\hat{\theta}(\mathbf{x})$  as in (4).

The training data  $(\boldsymbol{\theta}_i, \mathbf{x}_i)$ ,  $i = 1, \dots, m$ , for the first stage is obtained by sampling  $\boldsymbol{\theta}_i$  from the prior  $\pi(\boldsymbol{\theta})$  and time-series data  $\mathbf{x}_i$  from the implicitly defined  $p(\mathbf{x} | \boldsymbol{\theta}_i)$ . Throughout all experiments in this paper,  $m = 100,000$  and the data were split into 80,000 training and 20,000 validation examples.

In all simulations, we used the *same* training procedure and architecture for the convolutional neural network (called the “DireNet” — “dire” to indicate that we perform likelihood-free inference for dynamical models). The neural network consisted of two convolutional layers, the first followed by a max-pooling layer, and then a fully connected layer to capture long-range dependencies. We used rectified linear units (ReLU) as activation functions for these layers. ReLU activation functions are preferred over sigmoidal or hyperbolic tangent activation functions since they are less susceptible to vanishing gradients when training the neural network (e.g. Hochreiter 1998). For  $d$  dimensional model parameters  $\boldsymbol{\theta}$ , the output layer consisted of  $d$  output units, where we used the linear activation func-

tion. The detailed neural network architecture and training procedure is presented in the supplementary material.

The LFIRE objective in (2) was minimized using the R package glmnet (Friedman et al. 2010) as done before by Dutta et al. (2016). We also used the same settings as them: We used 1,000 data points from  $p(\mathbf{x})$  and  $p(\mathbf{x} | \boldsymbol{\theta})$ , and 10-fold cross-validation to select the  $L_1$  regularization strength  $\lambda$ .

LFIRE yields a surrogate posterior over the parameters  $\boldsymbol{\theta}$  (Dutta et al. 2016). If needed, samples from the posterior can be obtained by using it as the target distribution in any sampler. In this paper, however, sampling from the posterior was not necessary. The parameters  $\boldsymbol{\theta}$  are low-dimensional (as often the case in likelihood-free inference problems) so that posterior expectations were simply computed by taking weighted sums over a grid.

### 3 Inference for toy models

We illustrate and validate the proposed method on two toy models, and compare it to LFIRE with expert (manual) summary statistics and summary statistics defined by the deep network of Jiang et al. (2018).

#### 3.1 Models

The first model considered is the autoregressive conditional heteroscedasticity (ARCH) model defined by

$$x^{(t)} = \theta_1 x^{(t-1)} + e^{(t)}, \quad e^{(t)} = \zeta^{(t)} \sqrt{\alpha + \theta_2 (e^{(t-1)})^2} \quad (5)$$

with  $t = 1, \dots, 100$ ,  $x^{(0)} = 0$ ,  $\alpha = 0.2$ , and where  $\zeta^{(t)}$  and  $e_0$  are independent standard normal random variables. The parameters of interest are  $\boldsymbol{\theta} = (\theta_1, \theta_2)$  for which we assume a uniform prior on  $[-1, 1] \times [0, 1]$ . By forward simulating the above equations, we can easily sample time-series data  $\mathbf{x} = (x^{(1)}, \dots, x^{(100)})$  from the model. The exact posterior can be computed numerically to high accuracy (see e.g. Gutmann et al. 2018, Supplementary Material 1.2.4).

The second model considered is the moving average model of order two (MA2) which is described by

$$x^{(t)} = e^{(t)} + \theta_1 e^{(t-1)} + \theta_2 e^{(t-2)}, \quad x^{(0)} = e^{(0)} \quad (6)$$

where  $t = 1, \dots, 100$  and the  $e^{(t)}$  are independent standard normal variables. The parameters of interest are  $\boldsymbol{\theta} = (\theta_1, \theta_2)$ . We used as prior the uniform distribution on the triangle defined by  $\theta_1 \in [-2, 2]$ ,  $\theta_1 + \theta_2 > -1$ , and  $\theta_1 - \theta_2 < 1$  as Marin et al. (2012). We can again generate time-series data  $\mathbf{x} = (x^{(1)}, \dots, x^{(100)})$  from the model and the exact posterior can be computed numerically to high accuracy (see supplementary material).

MEASURE	DIRENET	JIANG ET AL
TRAIN $R^2$	<b>0.834</b>	0.782
TEST $R^2$	<b>0.827</b>	0.740
TRAIN MSE	<b>0.019</b>	0.028
TEST MSE	<b>0.020</b>	0.032

Table 1: ARCH model. Comparing the prediction accuracy of the DireNet and the deep net by Jiang et al. (2018). For  $R^2$ , larger is better; for MSE, smaller is better. The test set had size 100,000.

#### 3.2 Results

We first assess how well the DireNet can reconstruct the parameters  $\boldsymbol{\theta}$  from the raw data  $\mathbf{x}$ , that is how good the learned predictors  $\hat{\boldsymbol{\theta}}(\mathbf{x})$  are. We compare the reconstruction results with those for the deep neural network by Jiang et al. (2018) in terms of the mean-squared error and the coefficient of determination ( $R^2$ ),

$$R^2 = 1 - \frac{\sum_i \|\hat{\boldsymbol{\theta}}(\mathbf{x}_i) - \boldsymbol{\theta}_i\|_2^2}{\sum_i \|\boldsymbol{\theta}_i - \bar{\boldsymbol{\theta}}\|_2^2}, \quad (7)$$

where  $\boldsymbol{\theta}_i \sim \pi(\boldsymbol{\theta})$  and  $\mathbf{x}_i \sim p(\mathbf{x} | \boldsymbol{\theta}_i)$ . Table 1 shows that the proposed DireNet obtains a higher  $R^2$  value and a lower MSE on both the training and the test set, the latter of which indicating better generalization performance. It also shows that the gap between the training and the test performance is smaller for the DireNet, which indicates less overfitting. The reduction in overfitting is to be expected given the reduced number of parameters in the DireNet (8,422 vs. 30,502), but the better generalization and training performance indicates that using convolutional layers is beneficial for the time-series data.

Figure 1 shows example reconstructions  $\hat{\boldsymbol{\theta}}(\mathbf{x})$  obtained by the DireNet. Further examples and corresponding plots for the deep network by Jiang et al. (2018) are shown in the supplementary material. In the DireNet figures, the reconstructions for  $\mathbf{x} \sim p(\mathbf{x} | \boldsymbol{\theta})$  are clustered around  $\boldsymbol{\theta}$  (in blue) while the reconstructions for  $\mathbf{x} \sim p(\mathbf{x})$  (in red) are spread out over the domain of the prior as desired. We note that perfect reconstructions are not strictly necessary for LFIRE to work. This is because training of the classifier in LFIRE can accommodate systematic biases or distortions in the predictions  $\hat{\boldsymbol{\theta}}(\mathbf{x})$ ; for LFIRE to work, we only need that (sets of) predictions  $\hat{\boldsymbol{\theta}}(\mathbf{x})$  for different  $\boldsymbol{\theta}$  are distinguishable from one another (see supplementary material).

We next compare the accuracy of the inferred posteriors when using the DireNet, the deep network by Jiang et al. (2018), and manual expert summary statistics in

MODEL	DIRENET	JIANG ET AL	MANUAL
ARCH	<b>0.481</b> $\pm$ 0.017	0.959 $\pm$ 0.025	0.751 $\pm$ 0.046
MA2	<b>0.842</b> $\pm$ 0.025	1.631 $\pm$ 0.040	1.384 $\pm$ 0.041

Table 2: KL divergences between the exact posterior and the one learned by LFIRE with summary statistics given by the DireNet, the deep net by Jiang et al. (2018), and manual expert statistics. Averages  $\pm$  standard errors for 500 inference tasks are shown.

LFIRE. For the ARCH model, the expert statistics are auto-correlations and auto-covariances with lag up to order five as in (Dutta et al. 2016). For the MA2 model, we used auto-correlations with lag up to two as Marin et al. (2012). For all summary statistics, we included their pairwise combinations and a constant as features in LFIRE, so that all methods use the same model for the log-ratio. For all methods, LFIRE was used with a  $L_1$  penalty that prunes away unnecessary features.

For both models, we sampled 500 parameters from the prior  $\pi(\boldsymbol{\theta})$  and generated for each an observed data set  $\mathbf{x}^o$ , for which we then inferred the posterior  $p(\boldsymbol{\theta} | \mathbf{x}^o)$ . Since the exact posterior can be computed for both models (see above), we assessed the accuracy of the learned posterior by the Kullback-Leibler (KL) divergence between them. For its computation, we used a  $20 \times 20$  rectangular grid spanning the support of the prior.<sup>4</sup>

The results are summarized in Table 2. For both models, we see a significant improvement when using the DireNet as compared to both other approaches. Furthermore, in this case, the manually chosen statistics lead to better performance than the deep network when used in LFIRE. Example posteriors for the ARCH model are shown in Figure 2. Further examples are provided in the supplementary material.

## 4 Inference for complex models

We here apply our method to real-world models with intractable likelihoods and compare its performance to alternative methods.

### 4.1 Lotka-Volterra model

The Lotka-Volterra model is a continuous-time Markov chain that can be used to model predator-prey dynamics in ecology and chemical reactions (Boys et al. 2008). The generative process for the case of two

<sup>4</sup>The grid was the same for all methods and the numerical values of the KL divergences are reported up to the (common) stepsize.

species  $(x_1^{(t)}, x_2^{(t)})$  is defined by the transition distribution

$$p(x_1^{(t+\delta t)} = a_1, x_2^{(t+\delta t)} = a_2 | x_1^{(t)} = b_1, x_2^{(t)} = b_2) = \begin{cases} 1 - \gamma^{(t)}\delta t + o(\delta t) & \text{if } a_1 = b_1 \text{ and } a_2 = b_2 \\ \theta_1 b_1 \delta t + o(\delta t) & \text{if } a_1 = b_1 + 1 \text{ and } a_2 = b_2 \\ \theta_2 b_1 b_2 \delta t + o(\delta t) & \text{if } a_1 = b_1 - 1 \text{ and } a_2 = b_2 + 1 \\ \theta_3 b_2 \delta t + o(\delta t) & \text{if } a_1 = b_1 \text{ and } a_2 = b_2 - 1 \\ o(\delta t) & \text{otherwise} \end{cases}$$

where  $\gamma^{(t)} = \theta_1 b_1 + \theta_2 b_1 b_2 + \theta_3 b_2$ . The model has three parameters  $\boldsymbol{\theta} = (\theta_1, \theta_2, \theta_3)$  and for each we assume a uniform prior:  $\theta_1 \in [e^{-2}, 1]$ ,  $\theta_2 \in [e^{-5}, e^{-2.5}]$ , and  $\theta_3 \in [e^{-2}, 0]$ . We can sample from the model with the algorithm by Gillespie (1977), see also Fearnhead and Prangle (2012), and in our simulations, we use time-series  $\mathbf{x} = ((x_1^{(1)}, x_2^{(1)}), \dots, (x_1^{(50)}, x_2^{(50)}))$  of length fifty.

We compared the performance of the DireNet to LFIRE with manual summary statistics. The manual summary statistics were the  $x_1^{(t)}$  and  $x_2^{(t)}$  as in previous work where ABC was used for inference (e.g. Toni et al. 2009).<sup>5</sup> For the comparison, we generated 500 observed data sets by sampling “true” data generating parameters  $\boldsymbol{\theta}$  from the prior  $\pi(\boldsymbol{\theta})$  and then solved the 500 inference problems. Since the likelihood is intractable, we assessed the performance by the relative error between the estimated posterior means and the true data generating parameters as done in previous work (Dutta et al. 2016). We compute the relative error for each dimension  $i$  of  $\boldsymbol{\theta}$ , i.e.

$$\mathcal{RE}_i = \frac{|\mathbb{E}(\theta_i | \mathbf{x}^o) - \theta_i^{\text{true}}|}{|\theta_i^{\text{true}}|}. \quad (8)$$

The expectation was approximated by a weighted sum over a  $20 \times 20 \times 20$  rectangular grid covering the support of the prior.

Using the same observed data sets for both the DireNet and the manual summary statistics allowed us to perform a point-wise comparison between the two methods. Following Dutta et al. (2016), we used the 500 relative errors of both methods to estimate the distribution of their difference  $\Delta_i^{\text{rel}}$ ,

$$\Delta_i^{\text{rel}} = \mathcal{RE}_i^{\text{DireNet}} - \mathcal{RE}_i^{\text{Manual}}. \quad (9)$$

If the distribution is skewed to the left, the proposed approach performs better and vice-versa. Similarly, negative expected values of  $\Delta_i^{\text{rel}}$  indicate better performance of the proposed method.

Figure 3 shows the distribution for the three parameters. All distributions are skewed to the left and the

<sup>5</sup>With the quadratic expansion in LFIRE as before.

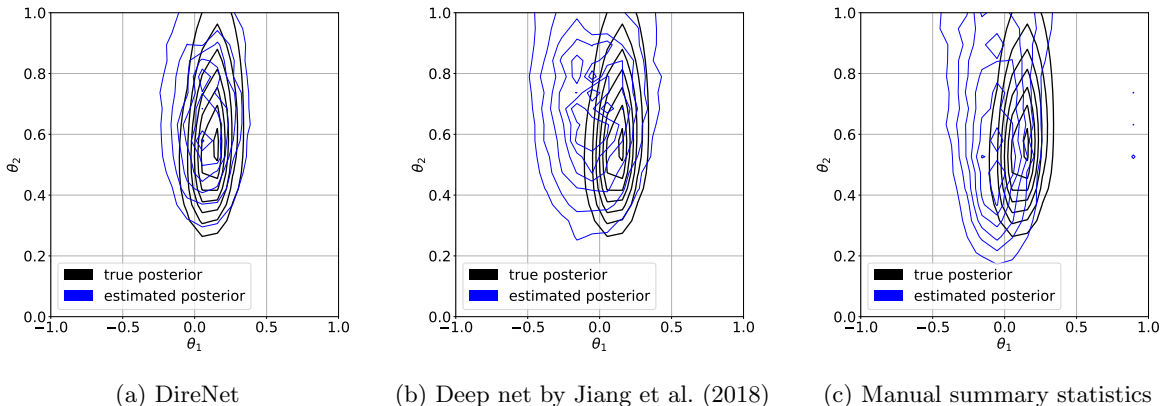


Figure 2: ARCH model: example posteriors for  $\mathbf{x}^o$  generated with  $\boldsymbol{\theta} = (0.3, 0.7)$ . Posteriors estimated by LFIRE are in blue, the exact (true) posterior is in black. (a-c) differ in the summary statistics used for LFIRE.

(bootstrap) 95% confidence intervals for the means are on the negative axis too. Together they indicate that the DireNet performs better than the manual statistics at estimating the parameters. The numerical values of the confidence intervals and further results are provided in the supplementary material.

## 4.2 Ricker model

The Ricker model (Ricker 1954) describes the observed size of an animal population over time. The dynamics of the population size is modeled as

$$\log N^{(t+1)} = \log r + \log N^{(t)} - N^{(t)} + \sigma e^{(t)}$$

where the  $e_t$  are independent standard normal random variables. We assume that we cannot observe the true population size but only a noisy measurement modeled as a sample from a Poisson distribution with mean  $\lambda_t = \phi N_t$  at time-steps  $t = 1, \dots, T$  (Wood 2010), with  $T = 50$ . The noisy observations are our data  $\mathbf{x}^o$  and we would like to infer the log growth rate  $\log(r)$ , the noise standard deviation  $\sigma$ , and the scaling parameter  $\phi$  of the observation model. As in previous work (Wood 2010), we assume uniform priors:  $\log(r) \in [3, 5]$ ,  $\sigma \in [0, 0.6]$  and  $\phi \in [5, 15]$ .

We compared our results with two other (non-LFIRE) inference methods — synthetic likelihood with the summary statistics by Wood (2010) and semi-automatic ABC by Fearnhead and Prangle (2012). The comparison is done in the same way as before for the Lotka-Volterra model (using again 500 inference tasks).

For the synthetic likelihood, we used the summary statistics and code provided by Wood (2010). Wood (2010) used fourteen summary statistics that included the coefficients of the autocorrelation function and the coefficients of fitted nonlinear autoregressive models

(see the supplementary material of Wood 2010). For the computation of the mean and covariance matrix that is needed in the synthetic likelihood approach, we used 1,000 model simulations. The posterior was then obtained by Markov Chain Monte Carlo using the same setup as Wood (2010) with the exception that we reduced the variances of the proposal distribution to 0.02, 0.01 and 0.05 for  $\log(r)$ ,  $\log(\sigma)$  and  $\log(\phi)$ , respectively, following Gutmann and Corander (2016) who observed better mixing with those values.

For the semi-automatic approach by Fearnhead and Prangle (2012), we used the code kindly provided by the authors. In brief, this approach transforms the summary statistics by Wood (2010) as well additional ones specified by the authors (the set “E2”) and then performs ABC by Markov chain Monte Carlo using the transformed summary statistics.

For the proposed method with LFIRE, we computed the posterior mean using a weighted sum over a  $20 \times 20 \times 20$  grid covering the prior while for the synthetic likelihood and semi-automatic ABC, it was computed by averaging the posterior samples.

Figure 4 shows the distributions of the difference in the relative errors comparing our approach to synthetic likelihood and semi-automatic ABC in the same way as in Figure 3. As before, distributions skewed to the left and negative expected values indicate better performance of the proposed method. We can see that for  $\log r$  and  $\phi$ , LFIRE with DireNet summary statistics leads to more accurate parameter estimates (posterior means) than the other two approaches. For  $\sigma$ , the results are not conclusive: The most likely outcome (mode of the distribution) is that the proposed method yields a more accurate estimate but bootstrap 95% confidence intervals on the mean include zero in case of the comparison to semi-automatic and are on

the positive axis in case of the comparison to synthetic likelihood. On the other hand, the 95% confidence intervals for the median are on the negative axis (see supplementary material). All in all, the differences for  $\sigma$  are not clear-cut, which may not be surprising given that  $\sigma$  is a difficult parameter to estimate (see e.g. the supplementary material).

### 4.3 Lorenz model

The Lorenz model of Wilks (2005) is a stochastic forty-dimensional time-series model for weather variables  $x_k^{(t)}$ ,  $k = 1 \dots 40$ . These follow a system of coupled stochastic differential equations:

$$\frac{\partial x_k^{(t)}}{\partial t} = -x_{k-1}^{(t)}(x_{k-2}^{(t)} - x_{k+1}^{(t)}) - x_k^{(t)} + F - g(x_k^{(t)}, \theta) + \eta_k^{(t)} \quad (10)$$

$$g(x_k^{(t)}, \theta) = \theta_1 + \theta_2 x_k^{(t)} \quad (11)$$

where  $F$  is a constant set to 10 and  $\eta_k^{(t)}$  a stochastic perturbation term representing unobserved variables of faster time scales (see Wilks 2005; Dutta et al. 2016). For negative  $k$  the model is cyclic, for example for  $k = 1$ ,  $k - 1 = 40$ . We follow the cited previous work and numerically solve the above equations for  $t \in [0, 4]$  using a 4th order Runge-Kutta solver discretizing the time interval into 160 time-steps, each of  $\Delta t = 0.025$ .

As in previous work, all initial values  $x_k^{(0)}$  are assumed known, and the parameters of interest are  $\theta = (\theta_1, \theta_2)$ . The prior for  $\theta$  was the uniform distribution on  $[0.5, 3.5] \times [0, 0.3]$ .

We used exactly the same DireNet as in all the other inference tasks before, thus taking only temporal convolutions. Since the time series is forty-dimensional, one could also have used spatio-temporal convolutions rather than just temporal ones further reducing the number of neural network parameters.

We compared the performance of the proposed method to LFIRE with the six manual summary statistics from Dutta et al. (2016), which were the mean; variance and auto-covariance with lag one of the  $x_k^{(t)}$  variables; the cross covariance with lag one of  $x_k^{(t)}$  with  $x_{k-1}^{(t)}$ ; and  $x_{k+1}^{(t)}$ , all averaged over all dimensions. The setup and analysis was as before for the Lotka-Volterra and Ricker model (using again 500 inference tasks).

The results are shown in Figure 5 (additional results with the numerical values for the bootstrap intervals, scatter plots showing true vs learned parameters, and example posteriors are in the supplementary material). There is a massive improvement over the manual summary statistics for both parameters. Indeed our ap-

proach outperforms here the manual summary statistics by the biggest margin, which may be due to the fact that time and experience of the research community has not yet optimized the manual summary statistics for this model in contrast to the Lotka-Volterra and Ricker model.

## 5 Conclusions

We considered the problem of learning summary statistics for likelihood-free inference by ratio estimation (LFIRE, Dutta et al. 2016), an approach that generalizes the synthetic likelihood method by Wood (2010); Price et al. (2017). We proposed to use parameter values predicted from raw data as summary statistics for LFIRE. Focusing on the important case of dynamical models and time-series data, we showed that convolutional neural networks are well suited to learn such summary statistics. On a wide range of different models, a *single* generic neural network architecture produced posterior estimates that are equally good or better than alternative, typically more customized, inference methods.

While we focused on time-series models, neural networks will likely provide suitable summary statistics for other large model classes too. For example, convolutional networks should be useful for data with spatial or spatio-temporal structure. Moreover, since LFIRE generalizes synthetic likelihood, our findings should also be useful for that approach.

The convolutional network only needs to be trained once per model and can then be deployed in arbitrarily many inference tasks (amortized inference). However, LFIRE requires solving an optimization problem for each parameter value for which we evaluate the posterior. While the outcome of the optimization can be stored and re-used for inference with different observed data sets, the repeated optimization is computationally costly. Importantly, however, this is an issue related to the current state of LFIRE and is not related to the method proposed in this paper. Techniques discussed and proposed in (Dutta et al. 2016) and (Cranmer et al. 2015) can be used to amend or alleviate this shortcoming, e.g. via transfer learning and Bayesian optimization (Gutmann and Corander 2016), and the proposed method can seamlessly be combined with these kinds of improvements.

Overall our results suggest that modern techniques for training neural networks are promising for likelihood-free Bayesian inference, and we expect that further drawing upon techniques from artificial intelligence will lead to further advances in this challenging area of statistics.

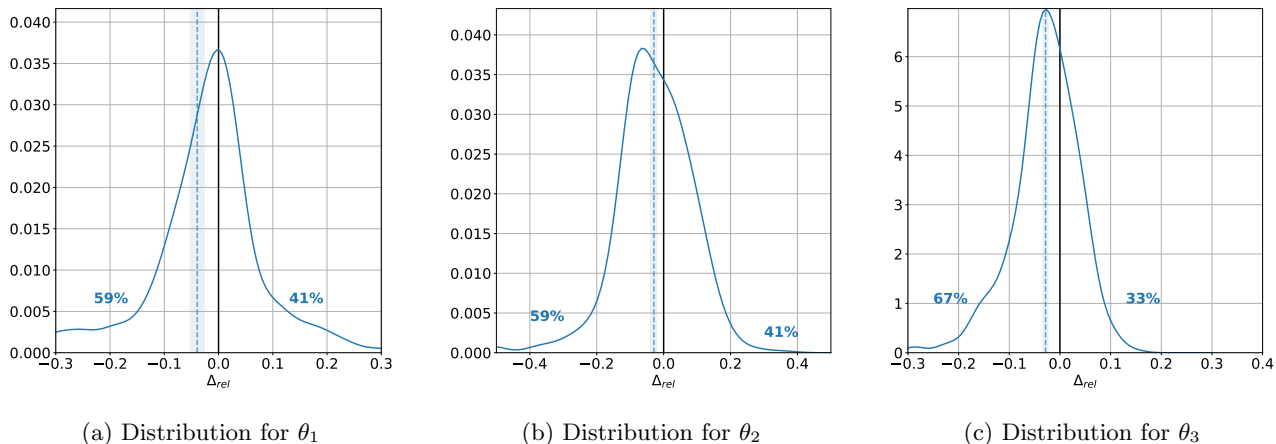


Figure 3: Lotka-Volterra model: Distribution of the difference between the relative error for the DireNet and manual summary statistics. Negative values correspond to better performance of the proposed method. Bootstrap 95% confidence intervals and mean are shaded in blue. The distributions are visualized as kernel density estimates with a Gaussian kernel (bandwidths for  $\theta_1$  to  $\theta_3$ : 0.025, 0.04, and 0.02).

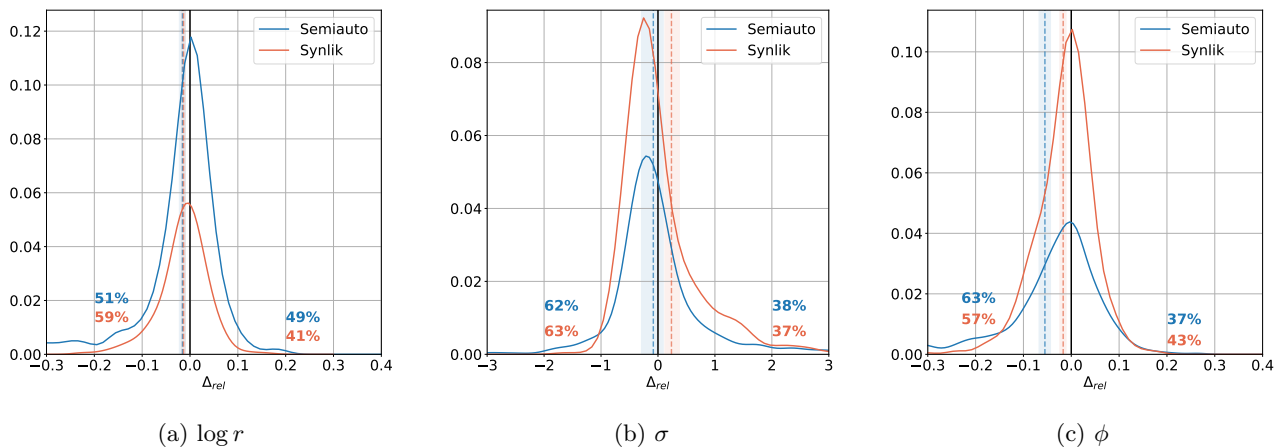


Figure 4: Ricker model: Distribution of the difference between the relative error for the DireNet and synthetic likelihood (red) and the DireNet and semi-automatic ABC (blue). Shown as above, bandwidths: 0.02, 0.2, 0.02.

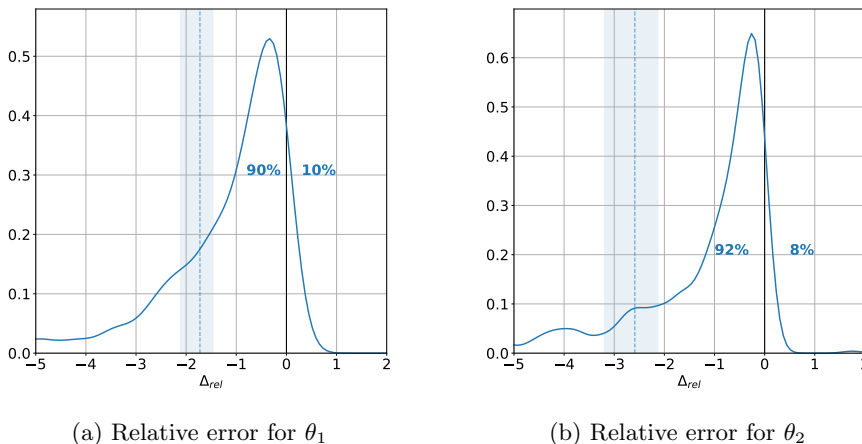


Figure 5: Lorenz model: Distribution of the difference between the relative error for the DireNet and manual summary statistics. Visualized as in Figure 3, bandwidths: 0.3 and 0.2.



## References

- [1] W. E. Ricker. Stock and recruitment. *Journal of the Fisheries Research Board of Canada*, 11(5): 559–623, 1954.
- [2] D. T. Gillespie. Exact stochastic simulation of coupled chemical reactions. *J. Phys. Chem.*, 81(25):2340–2361, December 1977.
- [3] P. J. Diggle and R. J. Gratton. Monte carlo methods of inference for implicit statistical models. *Journal of the Royal Statistical Society. Series B (Methodological)*, 46(2):193–227, January 1984.
- [4] C. Gouriéroux and A. Monfort. *Simulation-Based Econometric Methods (Core Lectures)*. Oxford University Press, 1996.
- [5] S. Tavaré, D. J. Balding, R. C. Griffiths, and P. Donnelly. Inferring coalescence times from dna sequence data. *Genetics*, 145(2):505–518, 1997.
- [6] S. Hochreiter. The vanishing gradient problem during learning recurrent neural nets and problem solutions. *Int. J. Uncertain. Fuzziness Knowl.-Based Syst.*, 6(2):107–116, 1998.
- [7] J. K. Pritchard, M. T. Seielstad, A. Perez-Lezaun, and M. W. Feldman. Population growth of human y chromosomes: a study of y chromosome microsatellites. *Molecular Biology and Evolution*, 16(12):1791–1798, 1999.
- [8] D. S. Wilks. Effects of stochastic parametrizations in the lorenz ’96 system. *Quarterly Journal of the Royal Meteorological Society*, 131(606): 389–407, 2005.
- [9] R. J. Boys, D. J. Wilkinson, and T. B. L. Kirkwood. Bayesian inference for a discretely observed stochastic kinetic model. *Statistics and Computing*, 18(2):125–135, 2008.
- [10] T. Toni, D. Welch, N. Strelkowa, A. Ipsen, and M. P. Stumpf. Approximate bayesian computation scheme for parameter inference and model selection in dynamical systems. *Journal of The Royal Society Interface*, 6(31):187–202, 2009.
- [11] M. Blum and O. Francois. Non-linear regression models for Approximate Bayesian Computation. *Statistics and Computing*, 20(1):63–73, 2010.
- [12] J. Friedman, T. Hastie, and R. Tibshirani. Regularization paths for generalized linear models via coordinate descent. *Journal of Statistical Software*, 33(1):1–22, 2010.
- [13] S. N. Wood. Statistical inference for noisy non-linear ecological dynamic systems. *Nature*, 466(7310):1102–1104, August 2010.
- [14] M. Gutmann and J. Hirayama. Bregman divergence as general framework to estimate unnormalized statistical models. In *Proceedings of the Conference on Uncertainty in Artificial Intelligence (UAI)*, 2011.
- [15] F. Hartig, J. M. Calabrese, B. Reineking, T. Wiegand, and A. Huth. Statistical inference for stochastic simulation models – theory and application. *Ecology Letters*, 14(8):816–827, 2011.
- [16] S. Aeschbacher, M. Beaumont, and A. Futschik. A novel approach for choosing summary statistics in approximate Bayesian computation. *Genetics*, 192(3):1027–1047, November 2012.
- [17] E. Cameron and A. N. Pettitt. Approximate bayesian computation for astronomical model analysis: a case study in galaxy demographics and morphological transformation at high redshift. *Monthly Notices of the Royal Astronomical Society*, 425(1):44–65, 2012.
- [18] P. Fearnhead and D. Prangle. Constructing summary statistics for approximate bayesian computation: semi-automatic approximate bayesian computation. *Journal of the Royal Statistical Society: Series B (Statistical Methodology)*, 74(3): 419–474, 2012.
- [19] J.-M. Marin, P. Pudlo, C. P. Robert, and R. Ryder. Approximate bayesian computational methods. *Statistics and Computing*, 22(6):1167–1180, 2012.
- [20] L. Prechelt. Early stopping — but when? In *Neural Networks: Tricks of the Trade*, Lecture Notes in Computer Science, pages 53–67. Springer, Berlin, Heidelberg, 2012.
- [21] M. Sugiyama, T. Suzuki, and T. Kanamori. Density-ratio matching under the bregman divergence: a unified framework of density-ratio estimation. *Annals of the Institute of Statistical Mathematics*, 64(5):1009–1044, 2012.
- [22] M. G. B. Blum, M. A. Nunes, D. Prangle, and S. A. Sisson. A comparative review of dimension reduction methods in approximate bayesian computation. *Statistical Science*, 28(2):189–208, 2013.
- [23] V. Mansinghka, T. D. Kulkarni, Y. N. Perov, and J. Tenenbaum. Approximate bayesian image interpretation using generative probabilistic graphics programs. In *Advances in Neural Information Processing Systems 26 (NIPS)*, 2013.
- [24] N. Srivastava, G. Hinton, A. Krizhevsky, I. Sutskever, and R. Salakhutdinov. Dropout: A simple way to prevent neural networks from overfitting. 15:1929–1958, 2014.

- [25] K. Cranmer, J. Pavez, and G. Louppe. Approximating likelihood ratios with calibrated discriminative classifiers. *arXiv:1506.02169*, June 2015.
- [26] S. Ioffe and C. Szegedy. Batch normalization: Accelerating deep network training by reducing internal covariate shift. In *PMLR*, pages 448–456, 2015.
- [27] D. P. Kingma and J. Ba. Adam: A method for stochastic optimization. In *International Conference on Learning Representations (ICLR)*, 2015.
- [28] R. Dutta, J. Corander, S. Kaski, and M. Gutmann. Likelihood-free inference by ratio estimation. *arXiv:1611.10242*, 2016.
- [29] M. Gutmann and J. Corander. Bayesian optimization for likelihood-free inference of simulator-based statistical models. *Journal of Machine Learning Research*, 17(125):1–47, 2016.
- [30] G. Papamakarios and I. Murray. Fast epsilon-free inference of simulation models with Bayesian conditional density estimation. In D. D. Lee, M. Sugiyama, U. V. Luxburg, I. Guyon, and R. Garnett, editors, *Advances in Neural Information Processing Systems 29*, pages 1028–1036. Curran Associates, Inc., 2016.
- [31] J. Corander, C. Fraser, M. Gutmann, B. Arnold, W. Hanage, S. Bentley, M. Lipsitch, and N. Croucher. Frequency-dependent selection in vaccine-associated pneumococcal population dynamics. *Nature Ecology & Evolution*, 1:1950–1960, 2017.
- [32] J. Lintusaari, M. Gutmann, R. Dutta, S. Kaski, and J. Corander. Fundamentals and recent developments in approximate Bayesian computation. *Systematic Biology*, 66(1):e66–e82, January 2017.
- [33] T. Lopez-Guevara, N. Taylor, M. Gutmann, S. Ramamoorthy, and K. Subr. Adaptable pouring: Teaching robots not to spill using fast but approximate fluid simulation. In S. Levine, V. Vanhoucke, and K. Goldberg, editors, *Proceedings of the 1st Annual Conference on Robot Learning (CoRL)*, volume 78 of *Proceedings of Machine Learning Research*, pages 77–86, 2017.
- [34] V. Ong, D. Nott, M.-N. Tran, S. Sisson, and C. Drovandi. Likelihood-free inference in high dimensions with synthetic likelihood. *QUT ePrints:112213*, 2017.
- [35] L. F. Price, C. C. Drovandi, A. Lee, and D. J. Nott. Bayesian synthetic likelihood. *Journal of Computational and Graphical Statistics*, pages 1–11, March 2017.
- [36] A. Tietäväinen, M. Gutmann, E. Keski-Vakkuri, J. Corander, and E. Haeggström. Bayesian inference of physiologically meaningful parameters from body sway measurements. *Scientific Reports*, 7(3771):1–14, 2017.
- [37] Z. An, L. South, D. Nott, and C. Drovandi. Accelerating Bayesian synthetic likelihood with the graphical lasso. *QUT ePrints:102263*, 2018.
- [38] B. Arnold, M. Gutmann, Y. Grad, S. Sheppard, J. Corander, M. Lipsitch, and W. Hanage. Weak epistasis may drive adaptation in recombining bacteria. *Genetics*, 208(3):1247–1260, January 2018.
- [39] M. Fasiolo, S. N. Wood, F. Hartig, and M. V. Bravington. An extended empirical saddlepoint approximation for intractable likelihoods. *Electron. J. Statist.*, 12(1):1544–1578, 2018.
- [40] D. Frazier, W. Maneesoonthorn, G. Martin, and M. B.P.M. Approximate bayesian forecasting. *International Journal of Forecasting*, in press, 2018.
- [41] M. Gutmann, R. Dutta, S. Kaski, and J. Corander. Likelihood-free inference via classification. *Statistics and Computing*, 28(2):411–425, 2018.
- [42] B. Jiang, T.-y. Wu, C. Zheng, and W. H. Wong. Learning summary statistic for approximate bayesian computation via deep neural network. *Statistica Sinica*, 2018.
- [43] S. Sisson, Y. Fan, and M. Beaumont. *Handbook of Approximate Bayesian Computation.*, chapter Overview of Approximate Bayesian Computation. Chapman and Hall/CRC Press, 2018.

# Supplementary Material

---

## A Neural networks

In total, we performed simulations with three different neural networks. In addition to the convolutional DireNet and the deep network by Jiang et al. (42) mentioned in the main text, we also performed simulations with a deep network similar to the one by Jiang et al. (42) but trained with modern techniques including Batch Normalization (26) and Dropout (24). This was done to have an additional baseline for comparison to the DireNet. In the following section we explore in more detail the effects of using each of those networks.

The three networks are shown in Figure 6. The output layers have either 2 or 3 neurons, depending on the model in question. For instance, for the ARCH model, we have two output parameters  $\theta = (\theta_1, \theta_2)$  and hence 2 neurons in the final layer. Excluding the output layer, the convolutional DireNet has 8,220 parameters, the deep network by Jiang et al. (42) 30,300, and the additional deep network 21,125 parameters. For the case of two outputs, the total number of parameters for the three networks become 8,422; 30,502; and 21,227.

Convolutional architectures have several hyperparameters per layer. For the convolutional layers, the *kernel* parameter is the size of the convolutional kernel, the *stride* parameter specifies how many units the kernel is shifted after each computation. We also have a number of these kernels, specified by the parameter *filter*. After the convolutional layers we have a *Flatten* layer that re-arranges the outputs so that fully-connected or *Dense* layers can accept them.

Throughout the paper we used 80,000 samples for training and 20,000 samples for validation. We trained the networks with the Adam optimizer (27) for 100 epochs using a batch size of 256 and early stopping with a patience of 30 epochs (20). The deep network uses batch normalization (26) and dropout for the hidden layers with standard dropout rate 0.5 (24). For DireNet, we used  $L_2$  regularization on the output layer with penalty strength set to the same value that Jiang et al. (42) used (namely 0.001).

## B Posterior for the moving average model

This section contains a derivation of the posterior distribution for the moving average model of order 2 (MA2). The derivation follows that of Gutmann et al. (41, Supplementary Material 1.2.4) with the addition of a second parameter, so that the model is parametrized by  $\theta = (\theta_1, \theta_2)$ .

The data generated by the model is a time-series  $\mathbf{x}_{1:T} = (x^{(1)}, \dots, x^{(T)})$ , which is defined as follows:

$$x^{(t)} = \epsilon^{(t)} + \theta_1 \epsilon^{(t-1)} + \theta_2 \epsilon^{(t-2)}, \quad x^{(0)} = \epsilon^{(0)}, \quad x^{(1)} = \epsilon_1 + \theta_1 \epsilon_0. \quad (12)$$

The  $\epsilon_t$  are standard normal variables. If we consider the (column) vector  $\boldsymbol{\epsilon} = (\epsilon_0, \dots, \epsilon_t)$  of all such variables, then  $\mathbf{x} = \mathbf{B}\boldsymbol{\epsilon}$ , where:

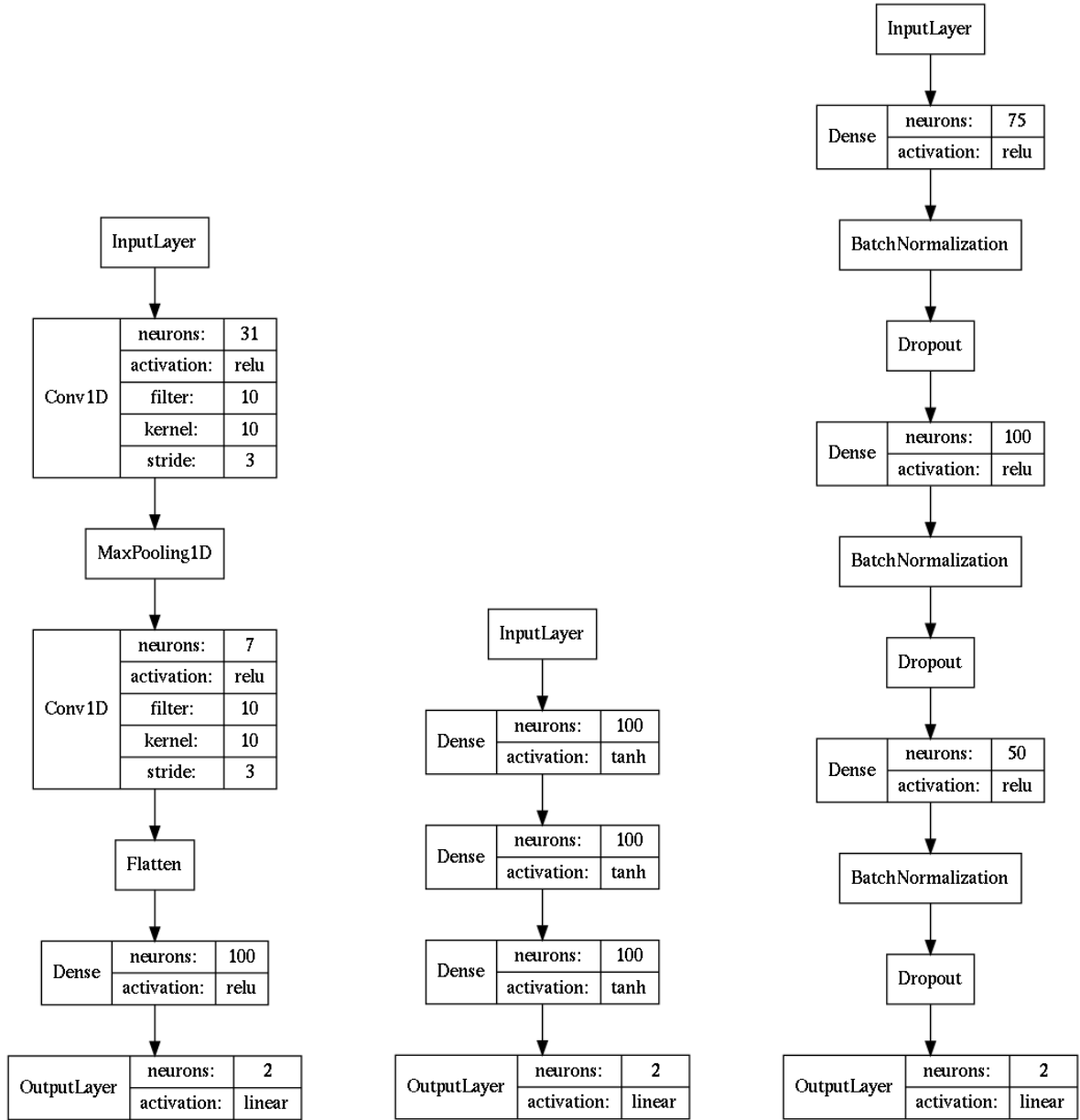
$$\mathbf{B} = \begin{pmatrix} 1 & 0 & 0 & 0 & \dots & 0 \\ \theta_1 & 1 & 0 & 0 & \dots & 0 \\ \theta_2 & \theta_1 & 1 & 0 & \dots & 0 \\ & & & \ddots & & \\ 0 & 0 & \dots & \theta_2 & \theta_1 & 1 \end{pmatrix} \quad (13)$$

We then know that  $\boldsymbol{\epsilon} \sim \mathcal{N}(\mathbf{0}, \mathbb{I})$  by definition above, where  $\mathbb{I}$  denotes the identity matrix. Hence:

$$\mathbf{x}_{0:T} \sim p(\mathbf{x}_{0:T} \mid \boldsymbol{\theta}) = \mathcal{N}(\mathbf{0}, \mathbf{B}\mathbf{B}^\top) \quad (14)$$

However, we do not observe  $x^{(0)}$ . Therefore we define the matrix  $\mathbf{M}$ , which is the matrix  $\mathbf{B}\mathbf{B}^\top$  with the first row and column removed. We thus know that:

$$\mathbf{x}_{1:T} \sim p(\mathbf{x}_{1:T} \mid \boldsymbol{\theta}) = \mathcal{N}(\mathbf{0}, \mathbf{M}) \quad (15)$$



(a) DireNet (convolutional network) (b) The network by Jiang et al. (42) (c) Additional deep neural network

Figure 6: Neural networks used. Compared to the network used in (42), the additional deep network that we considered has rectified linear activations and was trained with batch normalization and dropout. We also reduced the number of parameters by having less neurons in each hidden layer.

By using the definition of conditional probability, we obtain the posterior distribution of  $\theta$ ,

$$p(\theta \mid \mathbf{x}_{1:T}) = \frac{p(\mathbf{x}_{1:T} \mid \theta)}{p(\mathbf{x}_{1:T})} = \frac{p(\mathbf{x}_{1:T} \mid \theta)}{\int_{\theta} p(\mathbf{x}_{1:T} \mid \theta) \pi(\theta) d\theta}, \quad (16)$$

where  $\pi(\theta)$  denotes the prior of  $\theta$ .

## C Supplementary results

### C.1 ARCH model

For the ARCH model, we computed parameter predictions (reconstructions)  $\hat{\theta}(\mathbf{x})$  and posterior distributions for the three different neural network architectures mentioned above and for observed data generated with different values of  $\theta$ .

Figure 7 shows the predictions for the DireNet. As in Figure 1 in the main text, the whole parameter space is well covered by the predictions for  $\hat{\theta}(\mathbf{x})$  sampled from the marginal  $p(\mathbf{x})$  (in red) while the predictions for  $\mathbf{x}$  sampled from  $p(\mathbf{x} \mid \theta)$  are clustered around the particular value of  $\theta$  (in blue). Figure 8 shows the predictions for the deep network of Jiang et al. (42) in the same way. Comparing the two figures, we see that in Figure 8, the red points are less spread out and the blue points less concentrated than for the DireNet in Figure 7. Intuition suggests that the data clouds generated by the DireNet are more easily classifiable and hence the corresponding LFIRE posteriors also more accurate. This intuition is supported by the Kullback-Leibler divergences reported in the main text and the additional ones reported in Table 3.

Figure 12 shows the predictions with the additional deep network that we considered. We can here see that the predictions are poorer than for the two other neural networks. This is possibly due to the reduced flexibility (fewer neurons) of the network. The predictions are generally more concentrated (less spread-out), both for  $\mathbf{x} \sim p(\mathbf{x})$  and  $\mathbf{x} \sim p(\mathbf{x} \mid \theta)$ , than for the proposed DireNet. Table 3 shows that the corresponding posteriors are typically less accurate than those for the DireNet in line with our intuition. However, it also shows that, while less accurate than for the proposed DireNet, the posteriors are typically more accurate than those for the deep network by Jiang et al. (42). This is possibly due to all predictions being compressed into a smaller volume of the parameter space, and the subsequent training of the classifier in LFIRE being able to accommodate this systematic distortion as pointed out in the main text.

Example posteriors are shown in Figures 10 to 12. The true posterior, calculated numerically, is plotted in black for comparison. The figures show that the posteriors for the DireNet summary statistics match the true one typically better than the posteriors based on the other neural network summary statistics.

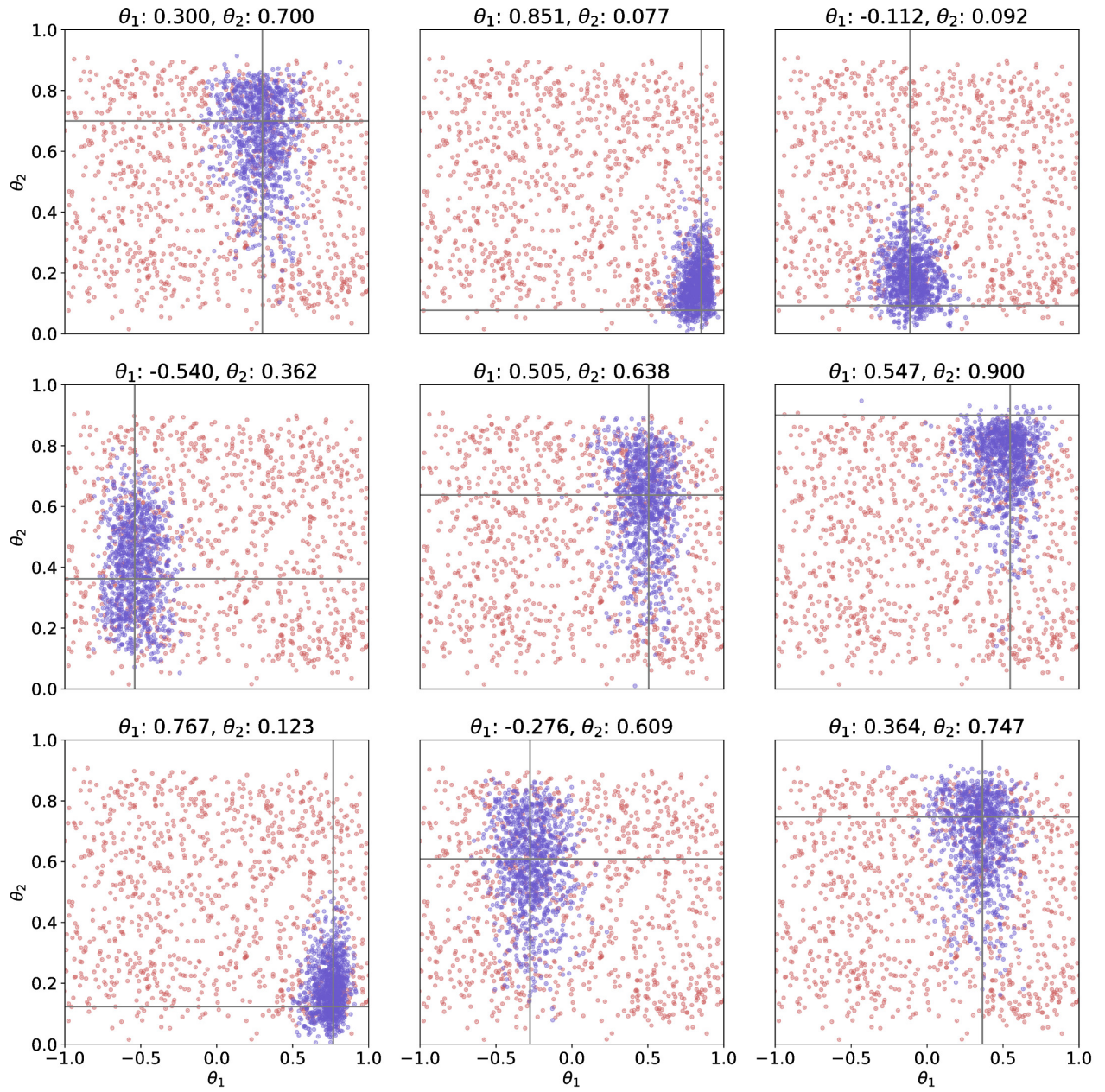
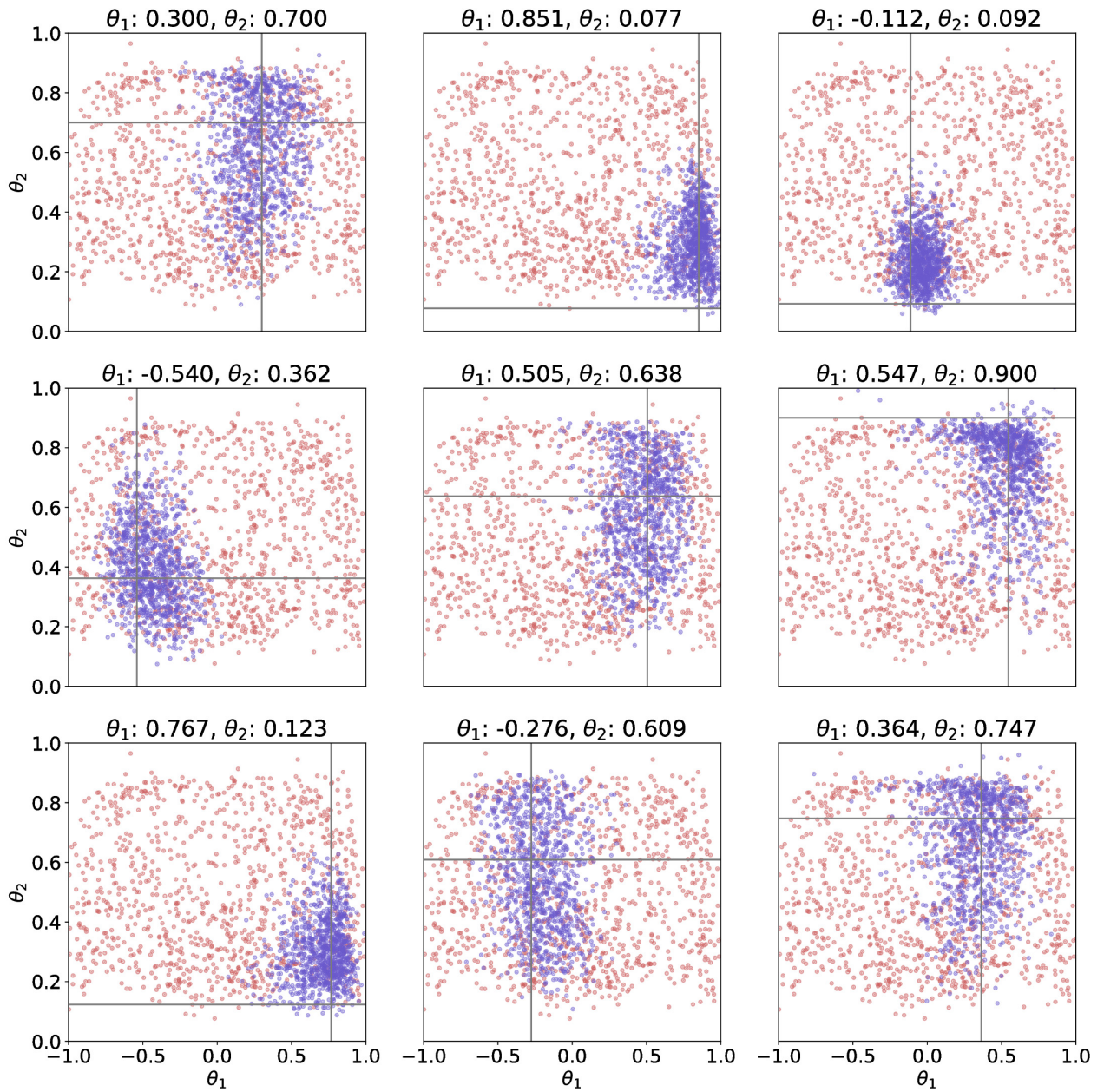
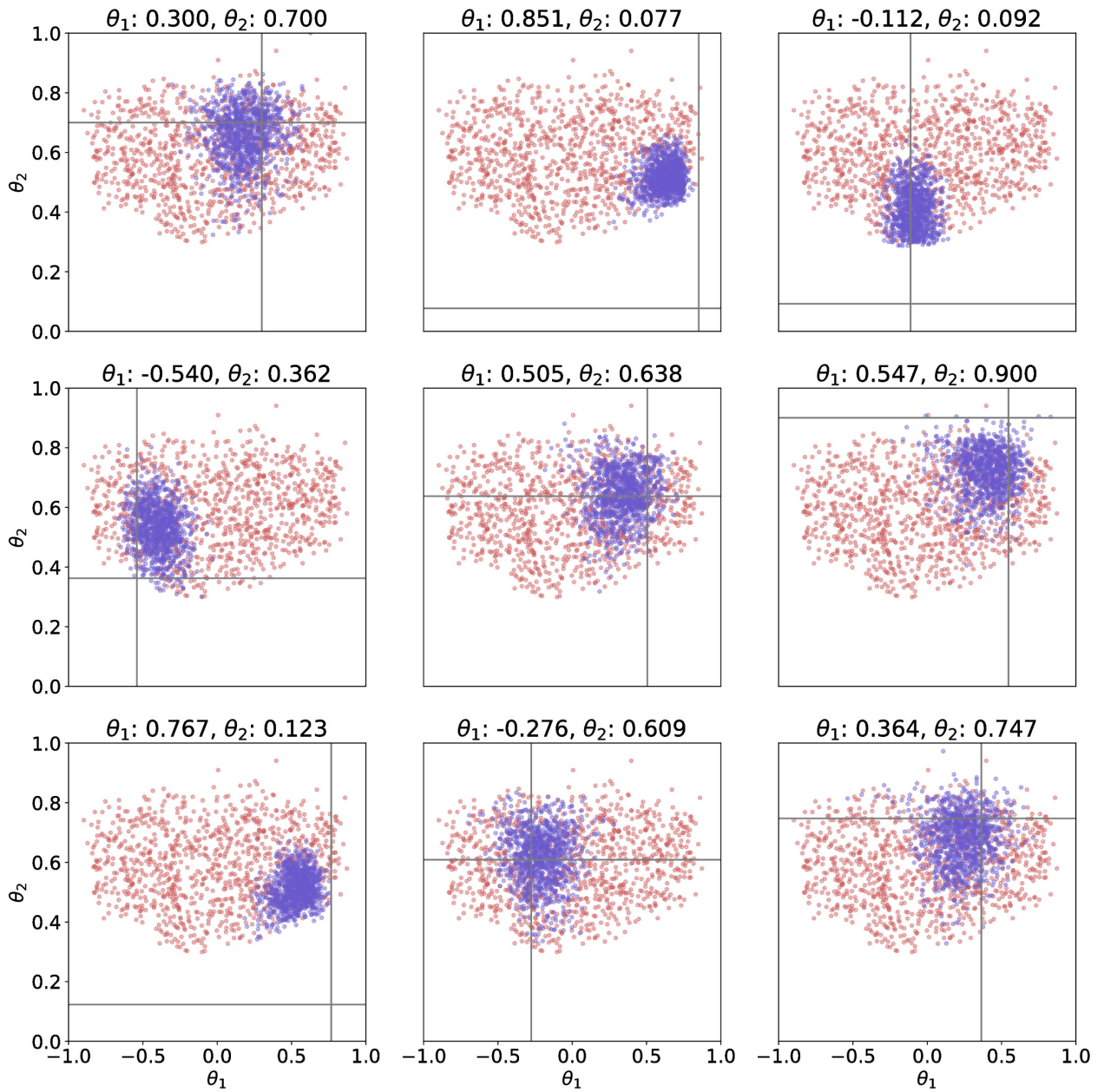


Figure 7: ARCH model: predictions  $\hat{\theta}(\mathbf{x})$  by the DireNet

Figure 8: ARCH model: predictions  $\hat{\theta}(\mathbf{x})$  by the deep network of Jiang et al. (42)

Figure 9: ARCH model: predictions  $\hat{\theta}(\mathbf{x})$  by the additional deep network



Theta	DireNet	Alt. Deep Net	Jiang et al. (42)
-1.000, 0.250	<b>0.393</b> $\pm$ 0.049	0.830 $\pm$ 0.105	0.840 $\pm$ 0.082
-1.000, 0.500	<b>0.503</b> $\pm$ 0.088	1.047 $\pm$ 0.112	1.059 $\pm$ 0.086
-1.000, 0.750	<b>1.018</b> $\pm$ 0.162	1.135 $\pm$ 0.108	1.203 $\pm$ 0.073
-0.333, 0.000	<b>0.287</b> $\pm$ 0.050	0.975 $\pm$ 0.120	0.951 $\pm$ 0.094
-0.333, 0.250	<b>0.343</b> $\pm$ 0.059	0.743 $\pm$ 0.128	0.887 $\pm$ 0.129
-0.333, 0.500	<b>0.673</b> $\pm$ 0.114	0.824 $\pm$ 0.086	0.889 $\pm$ 0.078
-0.333, 0.750	<b>0.508</b> $\pm$ 0.073	0.971 $\pm$ 0.164	1.006 $\pm$ 0.093
-0.333, 1.000	<b>0.751</b> $\pm$ 0.093	1.111 $\pm$ 0.125	1.102 $\pm$ 0.084
0.333, 0.000	<b>0.373</b> $\pm$ 0.113	0.705 $\pm$ 0.125	0.847 $\pm$ 0.115
0.333, 0.250	<b>0.411</b> $\pm$ 0.062	0.749 $\pm$ 0.094	0.753 $\pm$ 0.102
0.333, 0.500	<b>0.393</b> $\pm$ 0.042	0.869 $\pm$ 0.133	0.809 $\pm$ 0.116
0.333, 0.750	<b>0.695</b> $\pm$ 0.095	1.062 $\pm$ 0.103	0.943 $\pm$ 0.078
0.333, 1.000	<b>0.738</b> $\pm$ 0.094	1.013 $\pm$ 0.082	1.096 $\pm$ 0.084
1.000, 0.250	<b>0.698</b> $\pm$ 0.065	0.839 $\pm$ 0.094	1.185 $\pm$ 0.130
1.000, 0.500	<b>0.835</b> $\pm$ 0.041	0.970 $\pm$ 0.061	1.257 $\pm$ 0.064
1.000, 0.750	<b>1.044</b> $\pm$ 0.089	1.372 $\pm$ 0.120	1.452 $\pm$ 0.114

Table 3: ARCH model. Average KL divergence and standard errors over 20 runs for data sets generated with different values of  $\theta$ . The DireNet performs better than both other approaches. The KL divergence is computed between the true posterior and the estimated one.

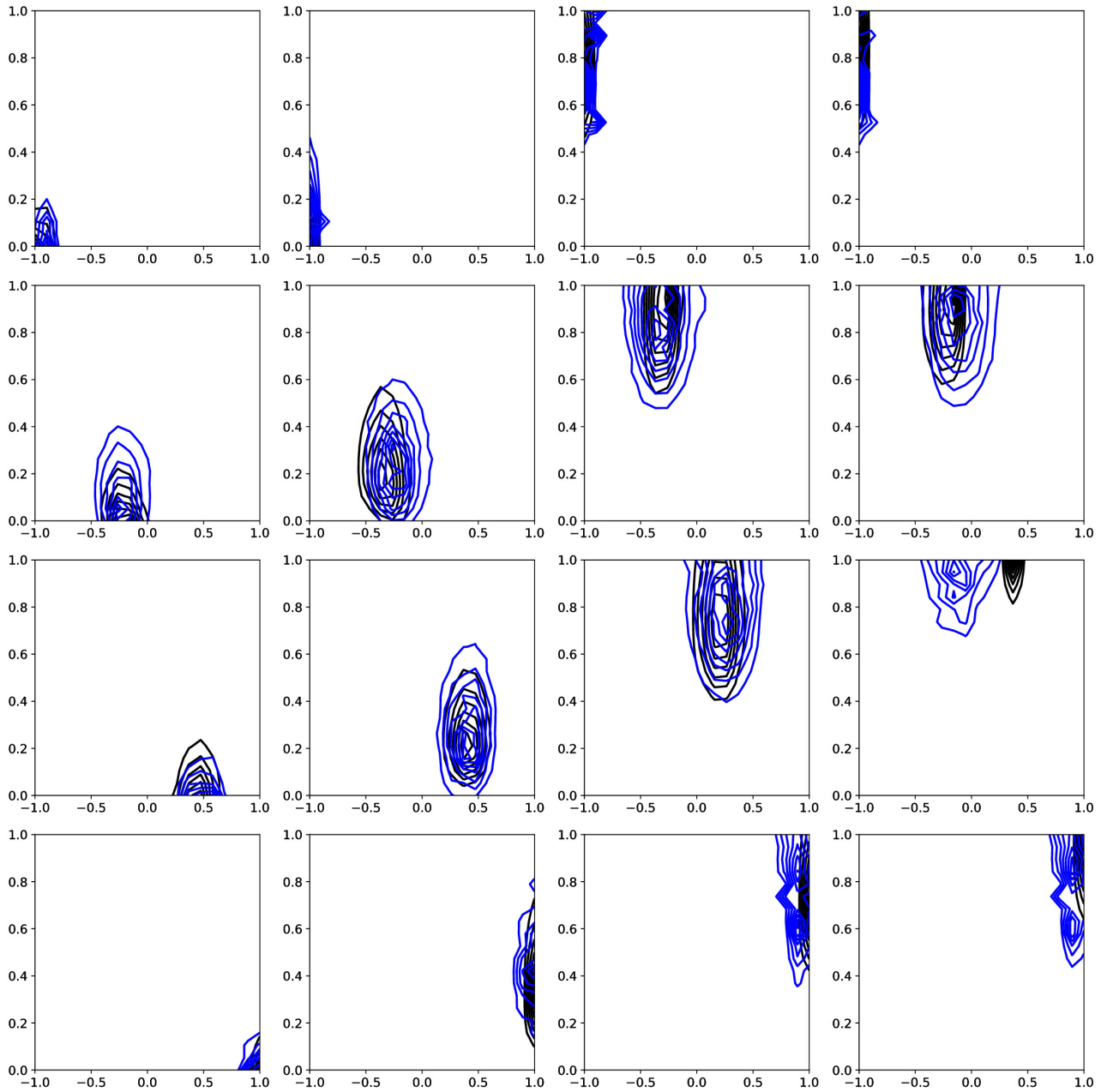


Figure 10: ARCH model: posteriors computed using the DireNet summary statistics.

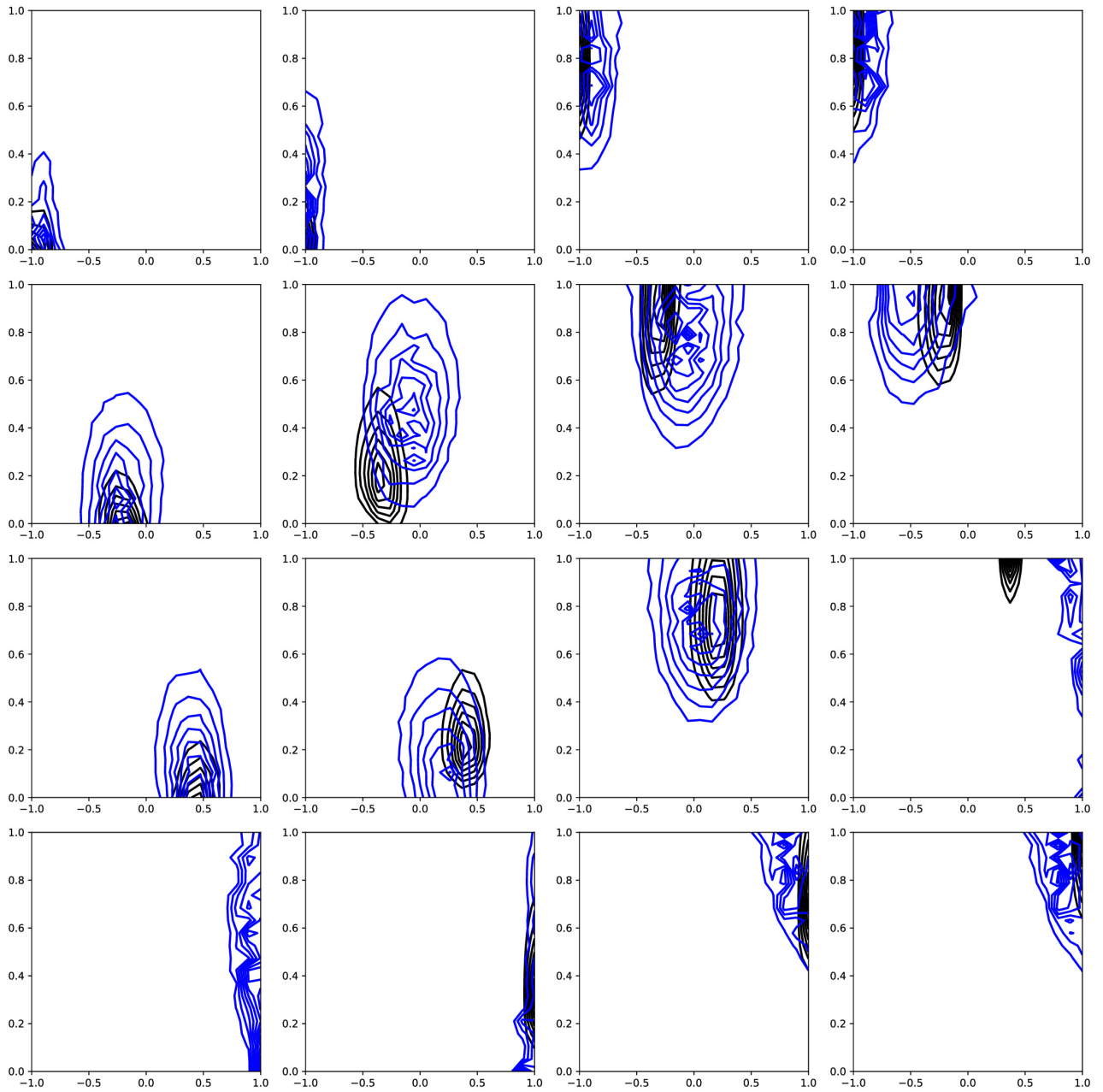


Figure 11: ARCH model: posteriors computed with summary statistics given by the deep network of Jiang et al. (42).

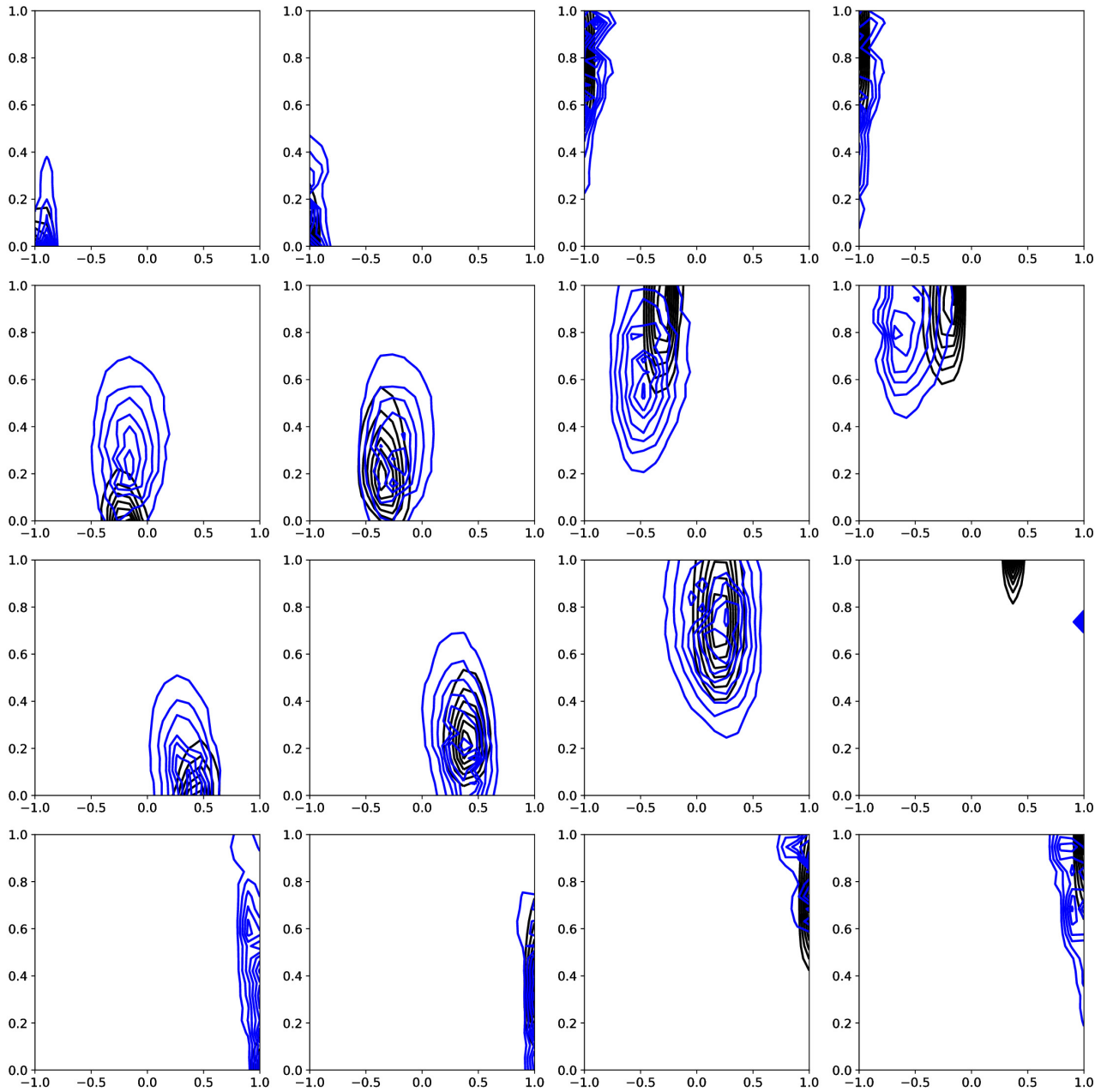


Figure 12: ARCH model: posteriors computed with summary statistics given by the additional deep network.

### C.2 Lotka-Volterra model

The lower and upper limit of the 95% confidence interval for the mean of  $\Delta_i^{\text{rel}}$  computed via bootstrapping, as well as the average of the bootstrap distribution of the mean is shown in Table 4. The results are based on 200 bootstrapped data sets (of size 500). The bootstrap confidence intervals are on the negative axis which indicates better performance of the proposed method (see main text).

Figure 13 plots true parameter values versus the posterior means for the 500 inference problems, when using the DireNet and the manual summary statistics in LFIRE. We see that the posterior means when using manual summary statistics are more over- or underestimated as compared to the case of the DireNet.

Parameter	Lower Limit	Upper Limit	Average
$\theta_1$	-0.052	-0.026	-0.039
$\theta_2$	-0.039	-0.020	-0.029
$\theta_3$	-0.034	-0.023	-0.028

Table 4: Lotka-Volterra model. Bootstrap distribution of the mean of  $\Delta_i^{\text{rel}}$ , showing the lower and upper limit of the 95% intervals as well as the average value.

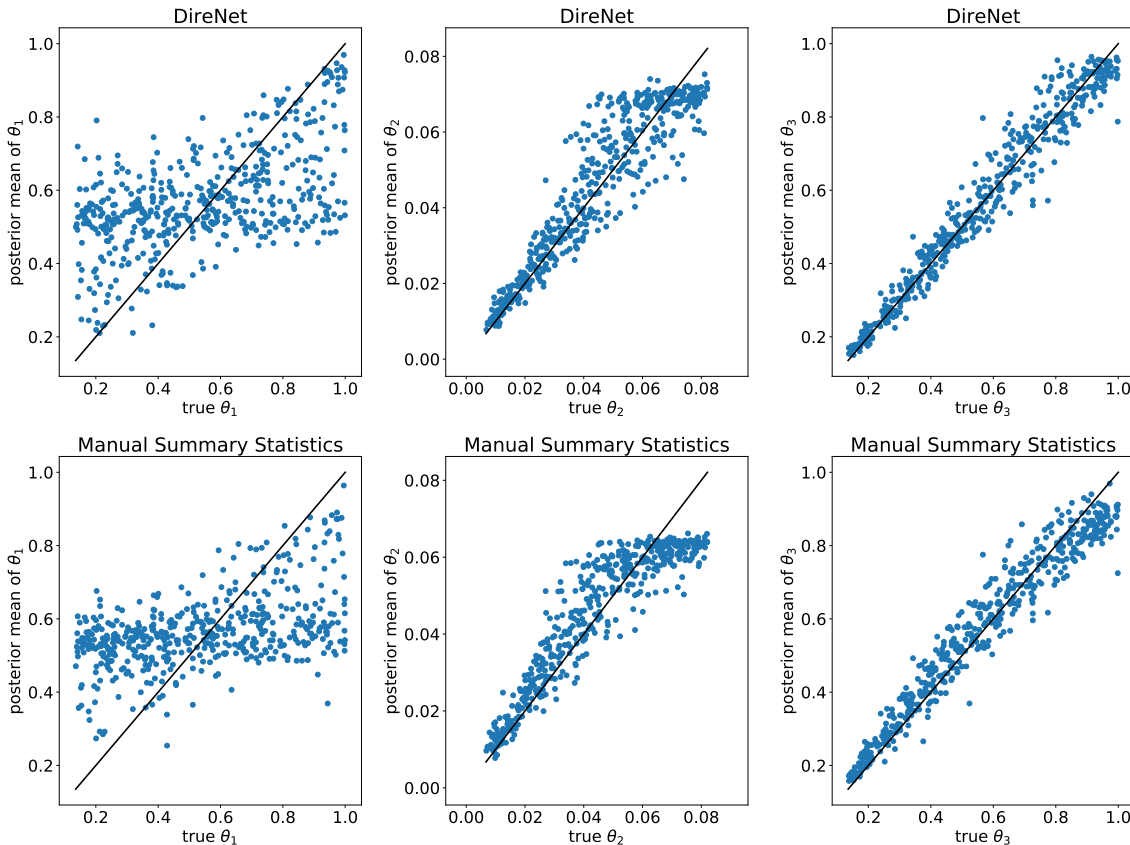


Figure 13: Lotka-Volterra model: true parameter values vs. posterior means comparing DireNet to manual summary statistics.

### C.3 Ricker model

We show in Tables 5 and 6 the bootstrap results for the comparison between LFIRE with the DireNet summary statistics and the synthetic likelihood with original summary statistics by Wood (13). For  $\sigma$ , the bootstrap confidence intervals for the mean of  $\Delta_i^{\text{rel}}$  is on the positive axis while for the median on the negative axis (see main text). Tables 7 and 8 shows the corresponding bootstrap results for the comparison to semi-automatic ABC (18). Here, the confidence interval for the median of  $\Delta_i^{\text{rel}}$  for  $\log r$  just includes zero while the corresponding interval for the mean is negative, which indicates a small difference in performance.

Figure 14 and Figure 15 plot the true parameters versus the posterior means for the different methods. In general, the scatter plots for LFIRE with the DireNet are more concentrated around the diagonal than the alternative methods, indicating better overall performance.

Parameter	Lower Limit	Upper Limit	Average
$\log r$	-0.018	-0.010	-0.014
$\sigma$	0.122	0.376	0.237
$\phi$	-0.024	-0.011	-0.017

Table 5: Ricker model: comparing LFIRE with the DireNet to *synthetic likelihood*. Bootstrap results for the mean of  $\Delta_i^{\text{rel}}$  computed as in Table 4.

Parameter	Lower Limit	Upper Limit	Average
$\log r$	-0.011	-0.006	-0.008
$\sigma$	-0.165	-0.103	-0.135
$\phi$	-0.011	-0.002	-0.007

Table 6: Ricker model: comparing LFIRE with the DireNet to *synthetic likelihood*. Bootstrap distribution of the median of  $\Delta_i^{\text{rel}}$ , showing the lower and upper limit of the 95% intervals as well as the average value.

Parameter	Lower Limit	Upper Limit	Average
$\log r$	-0.022	-0.009	-0.016
$\sigma$	-0.290	0.093	-0.082
$\phi$	-0.067	-0.043	-0.055

Table 7: Ricker model: comparing LFIRE with the DireNet to *semi-automatic ABC*. Bootstrap results for the mean of  $\Delta_i^{\text{rel}}$  computed as in Table 4.

Parameter	Lower Limit	Upper Limit	Average
$\log r$	-0.005	0.003	-0.001
$\sigma$	-0.193	-0.101	-0.147
$\phi$	-0.030	-0.013	-0.023

Table 8: Ricker model: comparing LFIRE with the DireNet to *semi-automatic ABC*. Bootstrap results for the median of  $\Delta_i^{\text{rel}}$  computed as in Table 6.

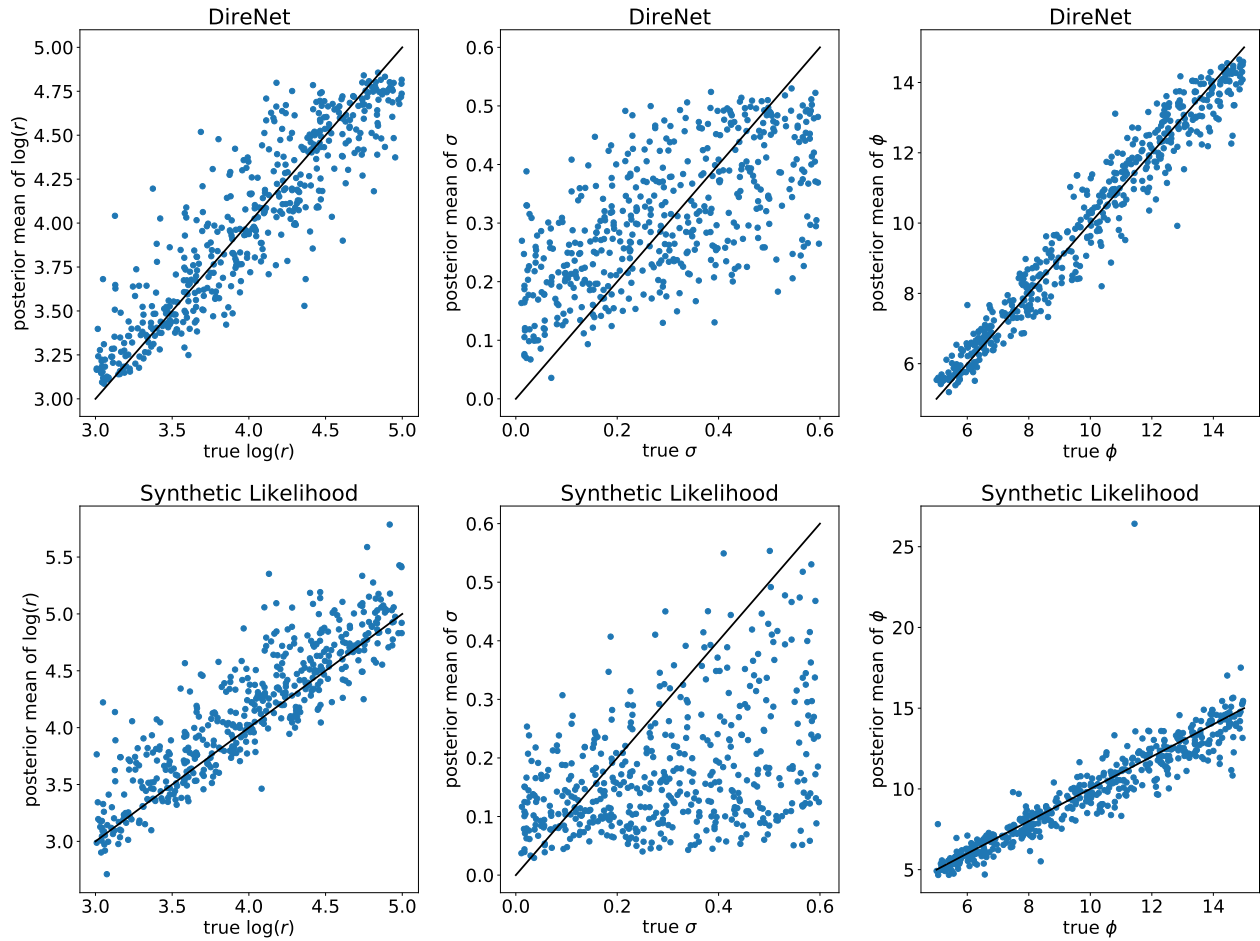


Figure 14: Ricker model: true parameter values vs. posterior means comparing LFIRE with DireNet to synthetic likelihood.

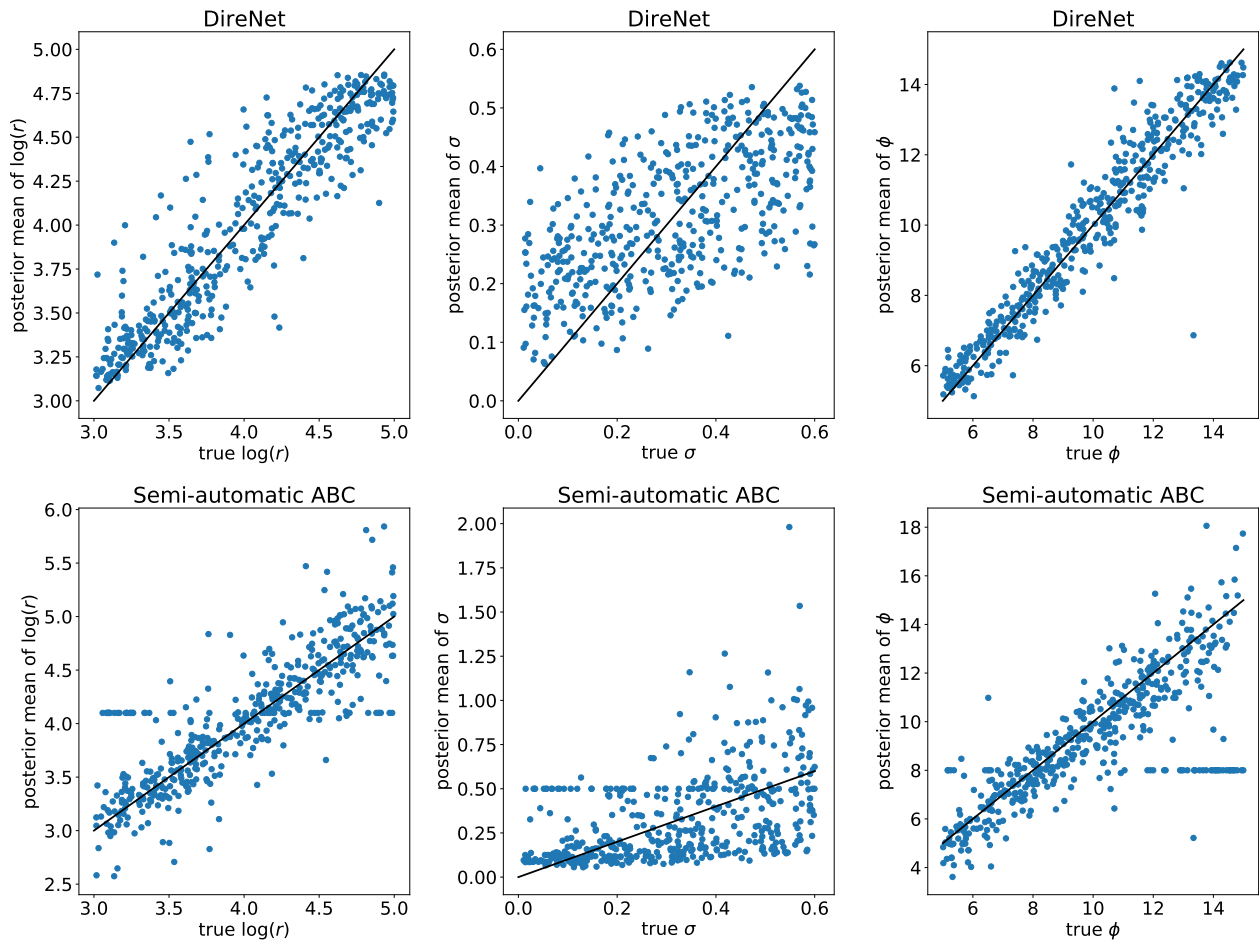


Figure 15: Ricker model: true parameter values vs. posterior means comparing LFIRE with DireNet to semi-automatic ABC.



C.4 Lorenz model

Table 9 shows the bootstrap results for the mean of  $\Delta_i^{\text{rel}}$ , and Figure 16 shows scatter plots of the true parameter value versus the posterior means. As mentioned in the main text, we see here a large improvement over the manual summary statistics. Given the large improvement, we also show in Figure 17 example posterior distributions. Previous work (28) showed the posterior for  $\theta = (2.0, 0.1)$  and our posterior with manual summary statistics matches their result well. Importantly, we see that when using DireNet, the posteriors are much tighter and centered close to true data generating parameter.

Parameter	Lower Limit	Upper Limit	Average
$\theta_1$	-2.116	-1.465	-1.725
$\theta_2$	-3.194	-2.126	-2.589

Table 9: Lorenz model: comparing DireNet to manual summary statistics. Bootstrap distribution for the mean  $\Delta_i^{\text{rel}}$  computed as in Table 4.

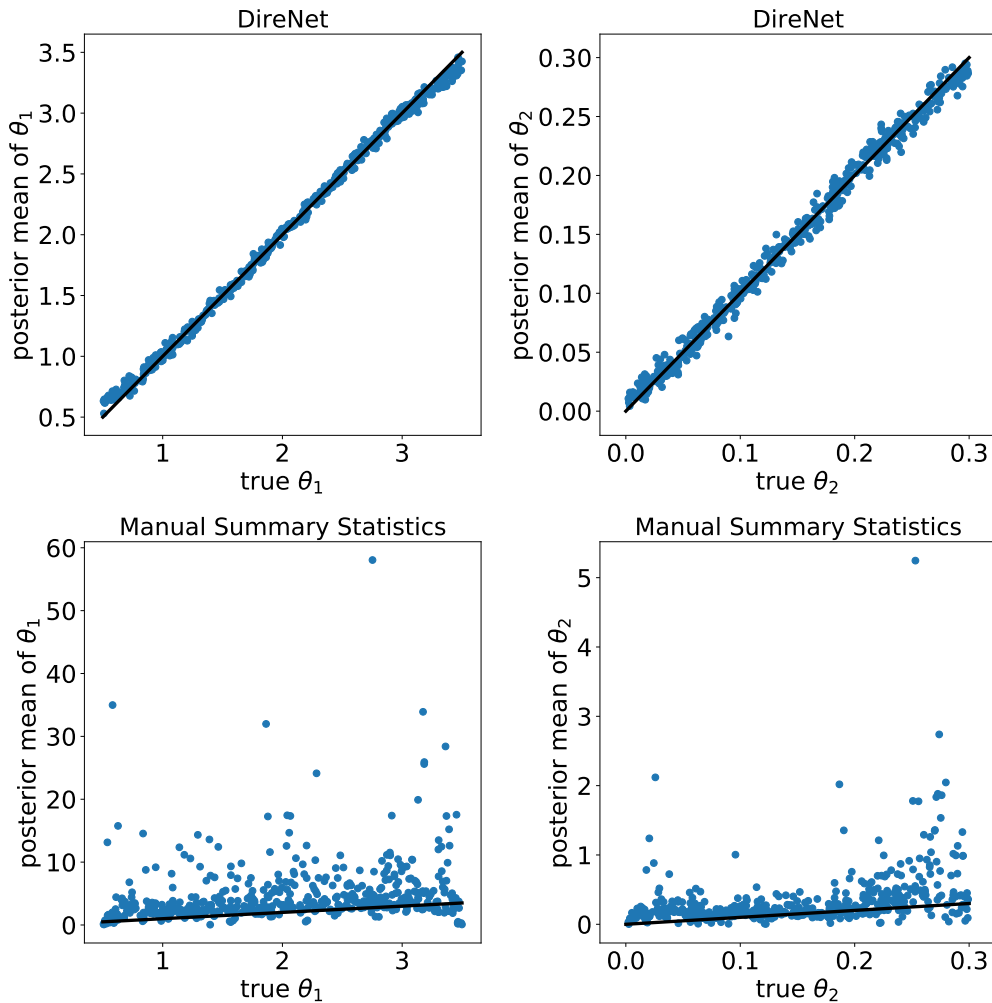
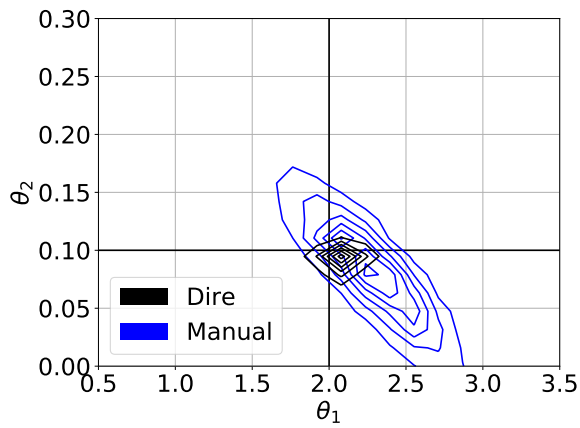
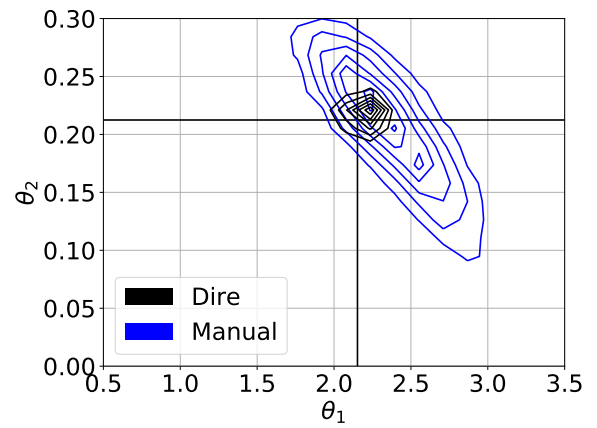


Figure 16: Lorenz model: true parameter values vs. posterior means comparing DireNet with manual summary statistics.



(a) Obs data generated with  $\theta = (2.0, 0.1)$



(b) Obs data generated with  $\theta = (2.152, 0.212)$

Figure 17: Lorenz model: posteriors for data sets generated with two different parameter values.